iScience

Article

Origin and development of uniparental and polyploid blastomeres

Graphical abstract

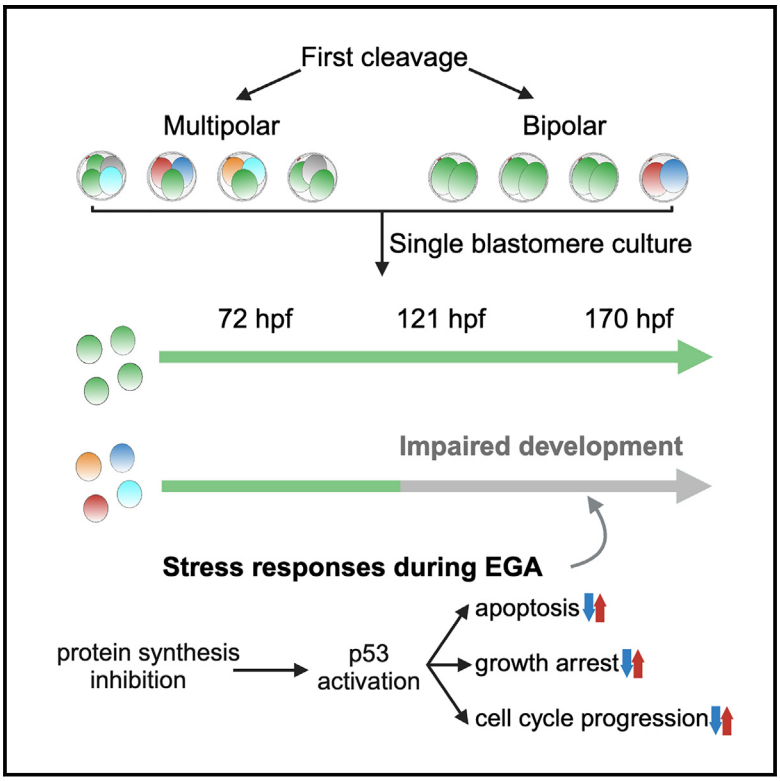

Highlights

- WG abnormal blastomeres arise from both multipolar and bipolar cleaving zygotes
- WG abnormal blastomeres exhibit impaired developmental potential
- WG abnormalities induce stress responses in gene expression during EGA
- WG abnormal cells may constitute an important contingent of embryos

Authors

Yan Zhao, Andrea Fernández-Montoro, Greet Peeters, ..., Katrien Smits, Ann Van Soom, Joris Robert Vermeesch

Correspondence

joris.vermeesch@kuleuven.be

In brief

Molecular biology; Omics

Zhao et al., 2025, iScience *28*, 112337
May 16, 2025
https://doi.org/10.1016/j.isci.2025.112337

CellPress

iScience

CellPress
OPEN ACCESS

Article

Origin and development of uniparental and polyploid blastomeres

Yan Zhao,[1,6,7] Andrea Fernández-Montoro,[2,7] Greet Peeters,[1] Tatjana Jatsenko,[1] Tine De Coster,[2] Daniel Angel-Velez,[2,3] Thomas Lefevre,[4] Thierry Voet,[4,5] Olga Tšuiko,[1] Ants Kurg,[6] Katrien Smits,[2] Ann Van Soom,[2] and Joris Robert Vermeesch[1,5,8,*]

[1]Laboratory for Cytogenetics and Genome Research, Department of Human Genetics, KU Leuven, 3000 Leuven, Belgium
[2]Department of Internal Medicine, Reproduction, and Population Medicine - Ghent University, 9820 Merelbeke, Belgium
[3]Research Group in Animal Sciences – INCA-CES, Universidad CES, Medellin 050021, Colombia
[4]Laboratory of Reproductive Genomics, Department of Human Genetics, KU Leuven, 3000 Leuven, Belgium
[5]KU Leuven Institute for Single Cell Omics (LISCO), University of Leuven, KU Leuven, Leuven, Belgium
[6]Department of Biotechnology, Institute of Molecular and Cell Biology, University of Tartu, 51010 Tartu, Estonia
[7]These authors contributed equally
[8]Lead contact
*Correspondence: joris.vermeesch@kuleuven.be
https://doi.org/10.1016/j.isci.2025.112337

SUMMARY

Whole-genome (WG) abnormalities, such as uniparental diploidy and triploidy, cause fetal death. Occasionally, they coexist with biparental diploid cells in live births. Understanding the origin and early development of WG abnormal blastomeres is crucial for explaining the formation of androgenotes, gynogenotes, triploidy, chimerism, and mixoploidy. By haplotyping 118 bovine blastomeres from the first cleavages, we identified that heterogoneic division occurs in both multipolar and bipolar cleaving zygotes. During heterogoneic division, parental genomes segregate into distinct blastomeres, resulting in the coexistence of uniparental and biparental diploid or polyploid cells. After culturing the totipotent blastomeres to three preimplantation stages and exploring transcriptomes of 446 cells, we discovered that stress responses contribute to developmental impairment in WG abnormal cells, resulting in either cell arrest or blastocyst formation. Their dominance in preimplantation embryos represents an overlooked cause of abnormal development. Haplotype-based screening could improve *in vitro* fertilization outcomes.

INTRODUCTION

Chromosomal abnormalities are common during human development, especially in the preimplantation phase.[1–3] One notable category of chromosome abnormalities are whole-genome (WG) anomalies.[4] Embryos bearing WG abnormalities contain abnormal levels of parental genomes rather than the normal diploid constellation with one maternal and one paternal haploid genome. For instance, uniparental haploid or diploid embryos carry only chromosomes from a single parent, whereas triploid embryos contain an additional haploid set of chromosomes from one of the parents. Constitutional WG anomalies are generally lethal during the embryonic stage. Triploidy occurs in approximately 1% of all conceptuses, contributing to around 10% of all spontaneous abortions[3,5] with extremely rare live-born cases surviving less than a year.[6] Complete and partial hydatidiform moles, occurring at rates of 1 in 1,000 and 3 in 1,000 pregnancies, respectively, are primarily androgenetic diploid and diandric triploid, respectively.[7] Mosaic forms with coexistence of normal cells can result in rare cases of live birth. For example, gynogenetic and androgenetic chimerism (coexistence of uniparental and normal cells) and diploid/triploid mixoploidy (coexistence of triploid and normal cells) have been reported in live-born individuals with congenital abnormalities.[8] As a model organism with a developmental process and an aneuploidy profile similar to that of humans,[9–11] WG abnormalities have also been identified at various stages during bovine development.[9,12–15]

Several models have been proposed to explain the mechanistic origins of WG abnormalities in embryos.[4] These include dispermy or diploid oocytes leading to triploidy, as well as parthenogenetic division of the oocyte or fertilization of an "empty" egg, resulting in uniparental embryos. Although these models explain the origin of triploid or uniparental embryos, they are limited by the deduction from surviving cells at later developmental stages. Additionally, the mechanistic origins of chimerism and mixoploidy remain speculative.[4,8] Since all body cells stem from a single zygote, diverse WG abnormalities observed during the late developmental stages are likely the result of irregular zygotic cleavages. Our recent study with bovine *in vitro* fertilized embryos provides direct evidence of a non-canonical first zygotic division as the mechanistic origin of cell lines exhibiting WG abnormalities,[15] which we termed "heterogoneic division." This specialized division involves the

segregation of entire parental genomes into distinct blastomeres, often triggered by polyspermy and occurring concurrently with multipolar zygotic division. Embryos following heterogoneic division typically contain blastomeres with diverse chromosomal constitutions, including biparental diploid, polyploid, and uniparental blastomeres, resembling those identified in chimeric and mixoploid individuals. Such cleavage involving WG segregation errors has also been reported in *in vitro* human and non-human primate embryos.[16,17]

Heterogoneic division, as the origin of blastomeres with WG abnormalities, represents a fundamental yet underexplored aspect of embryo development. Although research on preimplantation embryo development often focuses on aneuploidies and their implications,[18–20] there has been a lack of investigation into the developmental trajectory of spontaneously arising blastomeres carrying WG abnormalities. Examining the subsequent development of blastomeres following both heterogoneic and normal first zygotic divisions will provide valuable insights into the developmental disparities between blastomeres with WG abnormalities and normal blastomeres. Such insights are essential for advancing our understanding of the mechanistic origins of triploidy, moles, chimerism, and mixoploidy identified late during development and will guide genetic testing and embryo selection strategies regarding WG abnormalities.

Here, we explored the genome constitution and developmental potential of individual bovine blastomeres resulting from both bi- and multipolar first zygotic divisions. With haplotyping results of 118 blastomere outgrowths collected at three preimplantation stages, we demonstrated that uniparental and polyploid blastomeres arise from both multipolar and bipolar cleaving zygotes and exhibit a reduced blastocyst rate. Along with single-cell transcriptome analysis of 446 transcriptomes from blastomere outgrowths, we observed impaired transcriptomic development in WG abnormal cells, starting from major embryonic genome activation (EGA). For cells derived from outgrowths collected at the same time point, "impaired transcriptomic development" in WG abnormal cells means that their transcriptomes represent earlier stages of development compared to those with a normal genome constitution. This impaired development is attributed to stress responses induced in blastomere outgrowths with WG abnormalities during EGA. Despite these challenges, some blastomere outgrowths with WG abnormalities successfully managed this stress period and progressed to the blastocyst stage, underscoring their potential significant role in abnormal embryo development.

RESULTS

Whole-genome segregation errors occur in multipolar and bipolar first cleavages

To investigate the developmental program of gynogenetic/androgenetic and polyploid blastomeres following spontaneous heterogoneic division, we exploited the totipotency of blastomeres from early cleavage-stage embryos.[21,22] Following the first cleavage, 148 blastomeres from 52 bovine embryos (17 with bipolar and 35 with multipolar zygotic cleavage) were dissected and individually cultured to either day 2 (T1, 72 h post-fertilization (hpf), 4- to 6-cell stage), day 4 (T2, 121 hpf, 4- to 12-cell stage), or day 6 (T3, 170 hpf, blastocyst stage) post-blastomere splitting, respectively (Figure 1).

To determine the chromosomal constitution of the blastomeres in culture, we performed genome-wide haplotyping and copy-number profiling on cells derived from blastomere outgrowths using genotyping-by-sequencing (GBS)[23] (Figure 1). Of 148 blastomeres in culture from the 52 embryos, we successfully determined the chromosomal constitution of 118 blastomeres in culture from 43 embryos through haplotyping. Specifically, the chromosomal constitution was determined for all cultured blastomeres in 31 embryos, for a subset of cultured blastomeres in 12 embryos, and for none of the cultured blastomeres in 9 embryos (Figures 2A and 2B; Tables S1 and S2). Among these, 45% (n = 53) were identified as biparental diploid, whereas 41% (n = 48) exhibited WG abnormalities, including 35 androgenetic, 9 gynogenetic, 3 diandric triploid, and 1 triandric tetraploid blastomeres. Additionally, 14% (n = 17) of the blastomeres in culture with inferred chromosomal constitution were found to be anuclear. All anuclear blastomeres and the majority (96%, 46 out of 48) of blastomeres with WG abnormalities originated from embryos undergoing multipolar first cleavage (Figure 2B; Table S1).

For the 31 embryos with all blastomeres in culture successfully haplotyped, the genome composition of each blastomere allowed us to reconstruct genome segregation patterns during the first cleavage. The inference of the zygotic cleavage pattern was based on GBS haplotyping results, which enabled the identification of the parental and mechanistic origin, as well as the copy number of each chromosome. Additionally, whole-genome errors could be detected through distinct patterns across most of the genome,[23,24] Therefore, although speculative, the inferred genome segregation patterns are strongly supported by evidence from the haplotyping results. We observed three broad categories of genome segregation patterns during the first cleavage (Figure 2C; Table S1). Category 1 contains six embryos with all blastomeres harboring WG abnormalities. Category 2 comprises nine embryos with a mixture of blastomeres, some with WG abnormalities and others being biparental diploid. Category 3 consists of 16 embryos with only biparental diploid blastomeres. The four multipolar cleaving zygotes in this category also produced anuclear cells. Among the 31 fully examined embryos, 78% (14 out of 18) of those with multipolar first cleavage demonstrated heterogoneic division, whereas only 8% (1 out of 13) of embryos with bipolar first cleavage showed WG segregation errors (p = 0.00048; chi-squared test) (Figures 2C and 2D), confirming the enrichment of heterogoneic division in multipolar cleaving zygotes.[15] Furthermore, the high frequency of polyspermic conceptions in embryos undergoing multipolar first zygotic division and exhibiting WG segregation errors[15] was validated, with 86% (12 out of 14) of these embryos inferred to be fertilized by more than one sperm. In contrast, all other embryos with bipolar first cleavage or with multipolar first cleavage but without WG segregation errors were inferred to be fertilized by a single sperm (Figures 2C and 2D). Although less frequent, we observed two monospermic embryos showing heterogoneic division (Figure 2D), a phenomenon also observed in our previous studies.[13,15] Among these two, one exhibited bipolar genome segregation, resulting in one androgenetic blastomere, one

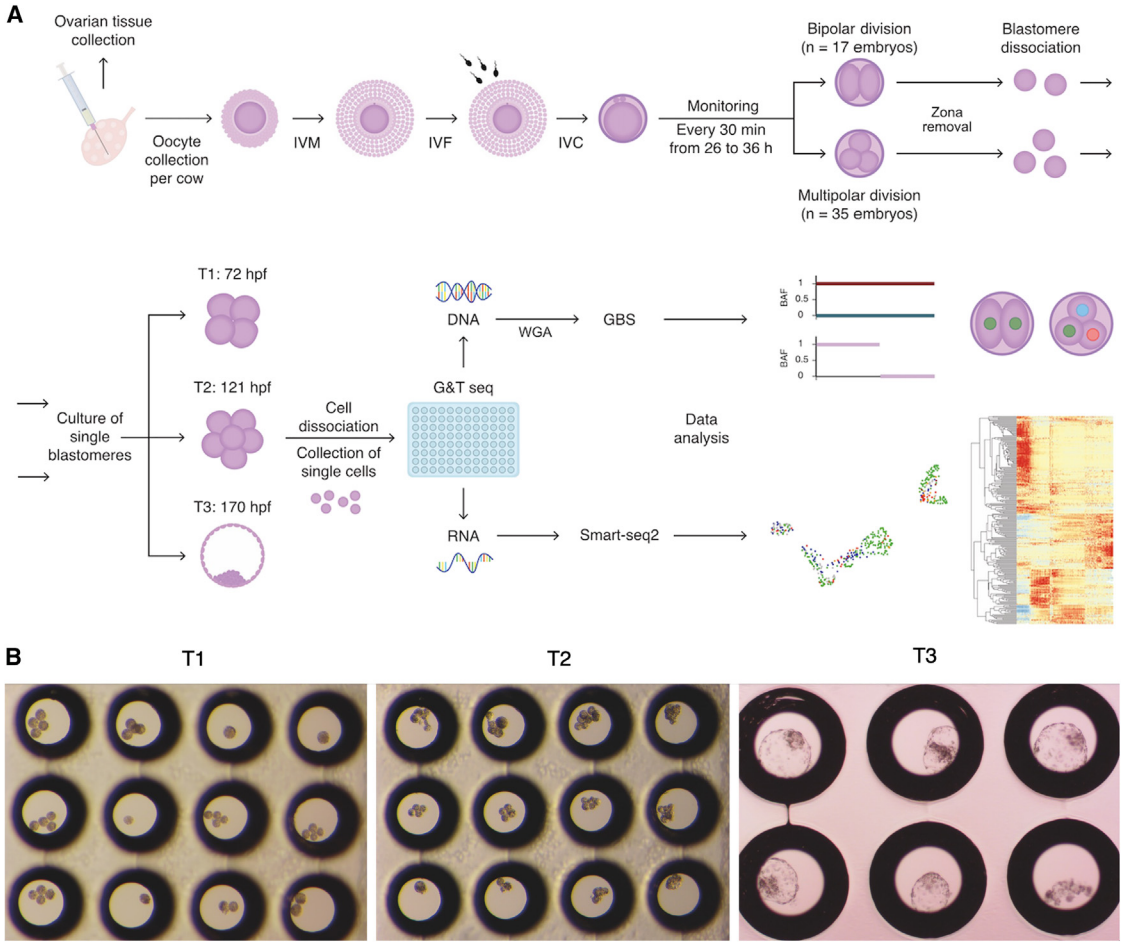

Figure 1. Experimental setup

(A) Diagram illustrating the experimental design. Bovine embryos were created and cultured *in vitro*. After the first zygotic division, blastomeres were dissected and cultured to three preimplantation time points. Blastomere outgrowths were subsequently collected and dissected into single cells. Each dissected cell underwent genome and transcriptome separation followed by sequencing. Genome data were used for haplotyping and copy-number profiling, whereas transcriptome data were used for gene expression analysis. Genome and transcriptome sequencing (G&T-seq): protocol for isolating poly(A) RNA and genomic DNA from single cells. Genotyping-by-sequencing (GBS): sequencing-based protocol for genome-wide haplotyping and copy-number profiling.

(B) Example images of blastomere outgrowths collected at T1, T2, and T3, respectively.

gynogenetic blastomere, and two anuclear blastomeres (shown in the second diagram of category 1 in Figure 2C). The other involved a tripolar spindle, segregating a haploid paternal and a haploid maternal genome into separate blastomeres, while both paternal and maternal haploid genomes were also segregated into a third blastomere. This resulted in one androgenetic blastomere, one gynogenetic blastomere, and one biparental diploid blastomere (illustrated in the fifth diagram of category 2 in Figure 2C). Notably, this second embryo aligns with the observation by Currie et al. of tripolar chromosome segregation in a normally fertilized embryo,[25] suggesting that the observed tripolar division may have involved WG segregation errors. Only 10% (1 out of 10) of dispermic embryos gave rise to triploid blastomeres, which is consistent with previous observations that dispermic fertilization seldom leads to triploid development.[15,26] Most of the observed mechanisms driving heterogoneic division align with those from our previous study.[13,15] Among the 15 embryos undergoing heterogoneic division, 10 were inferred to involve the extrusion of paternal pronuclei into separate cells, 4 likely involved an independent spindle separating paternal or maternal chromosomes, 2 likely involved a tripolar spindle, and 1 likely involved double spindles (Figure 2C).

Interestingly, two genome segregation mechanisms were newly identified. First, within category 1, we observed an embryo undergoing bipolar first cleavage, yet exhibiting heterogoneic division (Figure 2C). The most plausible explanation is that the two parental zygotic spindles failed to align and instead segregated into distinct blastomeres. Hence, genome-wide segregation errors are not confined to multipolar cleavers. Additionally, within category 3, we identified four embryos undergoing multipolar first cleavage, yet exhibiting normal genome segregation. Specifically, two biparental diploid blastomeres were generated alongside one or two anuclear cells (Figure 2C). These findings suggest that bipolar first cleavage does not always ensure

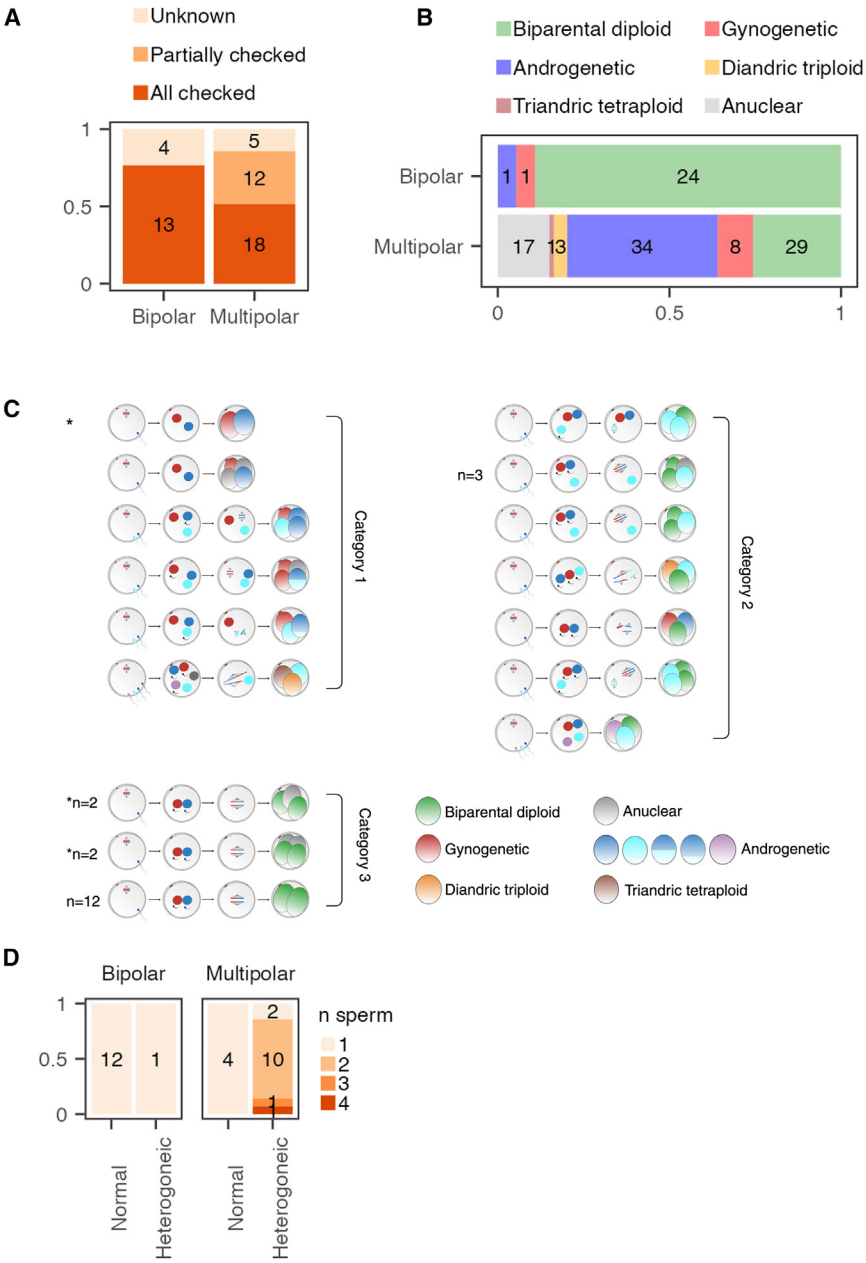

Figure 2. Whole-genome segregation errors occur in multipolar and bipolar first cleavages

(A) Numbers of bipolar and multipolar cleaving embryos used, categorized based on the completeness of embryo-derived blastomere outgrowth haplotyping: fully haplotyped (All checked), partially haplotyped (Partial), or not haplotyped (Unknown), with the y axis representing the fraction of counts.

(B) The inferred chromosomal constitution of 118 blastomeres in culture, with the x axis representing the fraction of counts.

(C) Three categories of genome segregation patterns identified during the first cleavage. In the oocyte being fertilized, the second meiotic division is depicted, along with the likely number of sperms fertilizing the embryo as deduced from the haplotypes. The arrows surrounding the pronuclei indicate replication occurred. During the first cleavage, spindles segregating the sister chromatids are shown. In the absence of a spindle, the genome is extruded. Numbers are given for patterns that occurred more than once. * in category 1 indicates the one embryo with bipolar first cleavage and WG segregation error. * in category 3 indicates the four embryos with multipolar first cleavage and without WG segregation error. For androgenetic blastomeres, different colors indicate genetic material from different sperm.

(D) Chromosomal segregation patterns for embryos with bipolar or multipolar first cleavage and the inferred number of sperm that fertilized the egg, with the y axis representing the fraction of counts. Normal: zygote cleaved without WG segregation error. Heterogoneic: zygote cleaved with WG segregation error. Bipolar and multipolar refer to embryos undergoing either bipolar or multipolar first cleavage, respectively. See also Tables S1 and S2.

normal genome segregation, and multipolar first cleavage does not inevitably result in WG or chromosomal segregation errors.

Blastomeres with whole-genome abnormalities can reach blastocyst stage despite impaired developmental potential

To investigate the developmental potential of heterogoneic-division-derived blastomeres with WG abnormalities, we compared the developmental stage of the 53 biparental diploid blastomere outgrowths and 48 blastomere outgrowths with WG abnormalities at the time of outgrowth collection (Figures 3A and 3B). We observed impaired development for blastomeres with WG abnormalities compared to biparental diploid blastomeres at T3, with 80% (12 out of 15) of biparental diploid blastomere outgrowths developing to blastocysts, whereas only 21% (6 out of 28) of blastomere outgrowths with WG abnormalities reached this stage (p = 0.0016; Fisher's exact test) (Figures 3B and 3C).

Since aneuploidy is known to affect embryo development, we next evaluated the impact of heterogoneic division on aneuploidy levels in daughter blastomeres. By comparing the aneuploidy spectrum of blastomeres from both normal genome segregation and heterogoneic division, we observed a lower proportion of euploid blastomeres and a higher proportion of blastomeres with high-level aneuploidy (defined as >10% of autosome regions being aneuploid, with 10% corresponding to two large chromosomes) in blastomeres from heterogoneic division, compared to blastomeres originating from zygotes with normal genome segregation (Figure S1). Specifically, for blastomeres with WG abnormalities resulting from heterogoneic division, 32% (10 out of 31) were euploid, whereas 55% (17 out

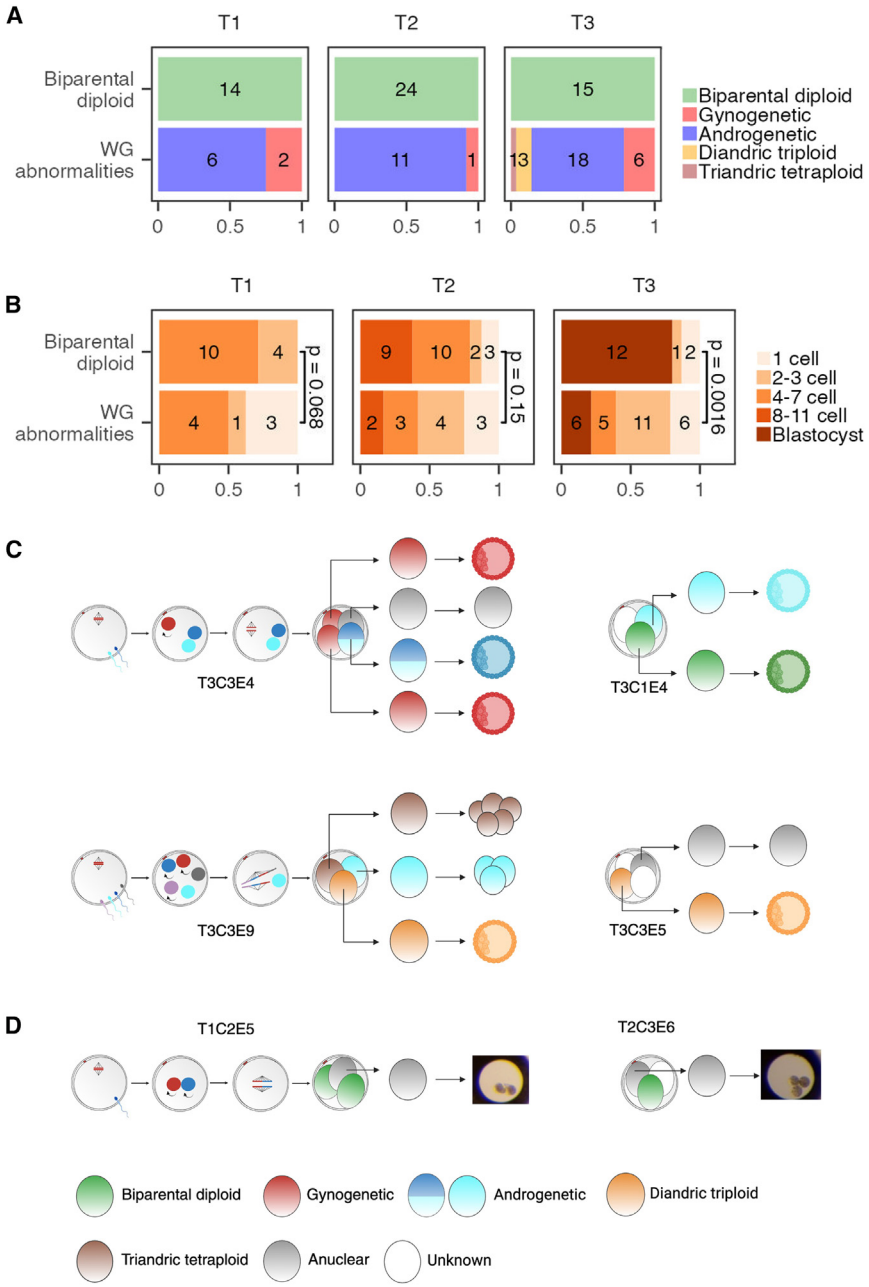

Figure 3. Blastomeres with whole-genome abnormalities can reach blastocyst stage despite impaired developmental potential

(A) Distribution of 53 biparental diploid blastomere outgrowths and 48 blastomere outgrowths with WG abnormalities across different time points of outgrowth collection, with the x axis representing the fraction of counts.

(B) Developmental stage comparison of biparental diploid blastomere outgrowths and blastomeres outgrowths with WG abnormalities in (A), with the x axis representing the fraction of counts (Fisher's exact test).

(C) Schematic representation of the six blastomere outgrowths with WG abnormalities that reached the blastocyst stage at T3, along with their sibling blastomere outgrowths and original embryos.

(D) Images of the two cleaved anuclear blastomere outgrowths and schematic diagrams illustrating the embryos from which they originated. In (C) and (D), the same symbols as in Figure 2C are employed. Fertilization and the first cleavage are not depicted for embryos containing blastomeres with an unknown haplotype (due to sample loss or haplotype failure). See also Figure S1 and Tables S1, S2, and S3.

of 31) displayed high-level aneuploidy. In contrast, for blastomeres from normal genome segregation, 56% (18 out of 32) were euploid, and only 3% (1 out of 32) exhibited high-level aneuploidy ($p = 6.3 \times 10^{-6}$; Fisher's exact test) (Figure S1). Similarly, other studies demonstrated the increased rate of complex chromosomal abnormalities for embryos with multipolar division.[16,27] The association between heterogoneic division and vulnerability to chaotic chromosomal missegregations might be caused by the spindle abnormalities implicated in this process[28](Figure 2C). To control for the effect of aneuploidy on blastomere development, we compared the development of only euploid blastomeres. At T3, all biparental diploid blastomere outgrowths (100%,12 out of 12) reached blastocyst stage, whereas a much lower proportion (36%, 4 out of 11) of blastomere outgrowths with WG abnormalities reached blastocyst stage (p = 0.0013; Fisher's exact test). Additionally, for androgenetic blastomere outgrowths collected at T3, 2 out of 15 containing the X chromosome reached the blastocyst stage, whereas the 3 without the X chromosome did not. This observation that only androgenetic blastomeres containing the X chromosome were able to develop into blastocysts is consistent with previous observations[29,30] and suggests that the Y chromosome alone is insufficient for blastocyst formation.

The majority of the 17 anuclear blastomeres were arrested at the one-cell stage. However, we identified two exceptions: one reached the two-cell stage at T1, and the other reached the three-cell stage at T2 (Figure 3D), suggesting that the cytoplasmic divisions could occur without a nucleus. Additionally, we identified 16 more anuclear biopsies from 14 non-anuclear blastomere outgrowths at various stages of development, with the majority of the original blastomeres (12 out of 14) from embryos that underwent multipolar first cleavage (Table S2). Hence, the formation of anuclear blastomeres is not restricted to the first zygotic division. To confirm the origin of these empty outgrowths/biopsies, we examined the mitochondrial genotypes for empty biopsies obtained from the same cows. Maternal inheritance of the

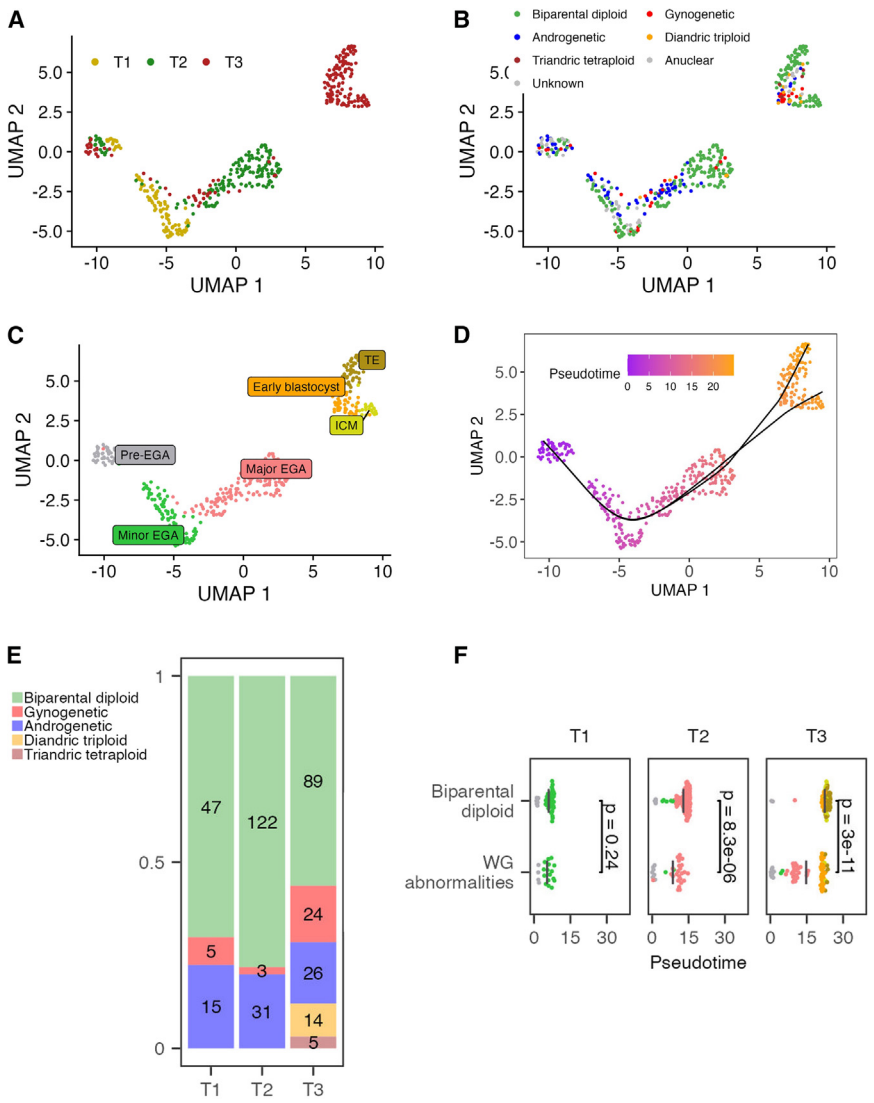

Figure 4. Whole-genome abnormalities do not alter the preimplantation developmental program but hinder transcriptomic development

UMAP for single-cell transcriptome data with cells colored by (A) time of outgrowth collection, (B) genome constitution, (C) and molecular developmental stage indicated by marker genes expression (D) pseudotime value inferred from trajectory analysis. The inferred pseudotime trajectories are indicated by black curved lines on the UMAP.

(E) The numbers of biparental diploid cells and cells with WG abnormalities used for transcriptome analysis for each time point, with the y axis representing the fraction of counts.

(F) Pseudotime comparison of biparental diploid cells and cells with WG abnormalities at each outgrowth collection time point [Student's t test; the numbers of biparental diploid cells and cells with WG abnormalities for each time point are shown in (E)]. Each dot represents one cell, with the x axis indicating its pseudotime value extracted from (D). Cells are colored according to their corresponding molecular developmental stage in (C) using the same color scheme. Vertical gray bars indicate the mean pseudotime value of each group. See also Figures S2–S4 and Table S2.

mitochondrial genome was corroborated by similar mitochondrial genotypes (Table S3).

To conclude, blastomeres with WG abnormalities from heterogoneic division show diminished development. Despite this, certain uniparental/polyploid blastomeres still progress to the blastocyst stage (Figure 3C), indicating their viability during the preimplantation stage and raising concerns about their further development and potential contribution to abnormal pregnancies.

Whole-genome abnormalities do not alter the preimplantation developmental program but hinder transcriptomic development

We hypothesized that the impaired development of blastomere outgrowths with WG abnormalities would be reflected in the transcriptomic profiles of constituent cells, with WG abnormalities potentially causing deviations in the preimplantation developmental program. To investigate the effects of WG abnormalities on transcriptomic development, we conducted single-cell transcriptome sequencing on 677 cells derived from collected blastomere outgrowths. Among these, 446 transcriptomes met our quality control criteria, 397 of which had corresponding haplotyping information (Table S2; STAR Methods). Before quality control, we noted significantly higher fractions of mitochondrial transcripts in cells from blastocyst stage outgrowths compared to cells from other stages, except the one-cell stage (Figure S2). The blastocyst stage cells with high fractions of mitochondrial transcripts were not enriched for cells with WG abnormalities. This finding suggests active mitochondrial gene expression in blastocysts and potential cytoplasmic RNA leakage in arrested one-cell stage outgrowths. Consistent with our findings, previous studies utilizing PCR analysis have demonstrated a significant increase in mitochondrial transcripts at morula and blastocyst stages across various mammalian species.[31–33]

Following dimensionality reduction with Unified Manifold Approximation and Projection (UMAP), single-cell gene expression profiles exhibited a developmental trajectory from T1 to T3 (Figure 4A). Cells with WG abnormalities did not form distinct clusters (Figure 4B). Instead, by checking the expression of marker genes for essential preimplantation stages, we identified clusters corresponding to minor EGA, major EGA, inner cell mass (ICM), and trophectoderm (TE) stages, which we define as the molecular developmental stages of the cells. The cell cluster without EGA (pre-EGA) contained cells arrested before EGA

(Figures 4C and S3). Pseudotime analysis with single-cell transcriptome data inferred developmental trajectories pointing to ICM and TE (Figure 4D). These results indicate that transcriptomic changes are mainly driven by the natural developmental program rather than variations in genome constitution, aligning with previous single-cell transcriptome analyses of uniparental[34] and aneuploid[19] cells from human preimplantation embryos.

We then explored whether the impaired development of blastomeres exhibiting WG abnormalities was reflected in single-cell transcriptome profiles. We characterized the physical age of the cells based on the time of outgrowth collection, whereas their molecular age was assessed using pseudotime values along the transcriptional trajectory. Compared to cells from biparental diploid outgrowths, those from outgrowths displaying WG abnormalities exhibited impaired development at T2 and T3, as evidenced by their smaller transcriptome-pseudotime ages (Figures 4E and 4F; $p = 8.3 \times 10^{-6}$ for T2 and $p = 3 \times 10^{-11}$ for T3; Student's t test). This trend persisted when considering only cells inferred to be euploid ($p = 0.023$ for T2 and $p = 0.00012$ for T3; Student's t test). Our observation indicates impaired transcriptomic development at the cell level in blastomeres with WG abnormalities starting from T2, coinciding with major EGA.

Some blastomere outgrowths collected at T2 or T3 did not have the expected number of cells and appeared to be cleaving more slowly or blocked in their development. Surprisingly, when mapping the transcriptome profiles onto the developmental trajectories, we observed that some cells from one-cell and two- to three-cell stage outgrowths at T3 displayed profiles resembling major EGA, whereas some cells from 4- to 7-cell outgrowths exhibited profiles akin to TE or ICM (Figure S4). These observations suggest that transcriptomic development can continue in the absence of cell divisions.

Distinct preimplantation cellular states are governed by specific key transcription factors

Since cells were clustered according to their molecular developmental stage regardless of genome composition, we next aimed to uncover the specific gene regulatory networks (GRNs) shaping cellular identity at each stage. We used pySCENIC to infer GRNs from single-cell RNA-seq data, based on co-expression of TFs and their target genes as well as *cis*-regulatory motif analysis. This approach identified 237 regulons, each comprising a transcription factor (TF) alongside its predicted target genes. Subsequently, we generated a UMAP visualization based on regulon activity, partitioning cells into distinct regulatory states (Figure 5A). As anticipated, cells belonging to the same molecular stage exhibited clustering, indicative of stage-specific regulatory dynamics. To further investigate the coactivity of TF combinations within each stage, we ordered cells based on their molecular stage and pseudotime values on the regulon activity heatmap. The resulting plot revealed stage-specific regulatory states characterized by the activation or repression of specific TFs (Figure 5B). We then selected key regulons with both high activity and specificity for each stage (Figures 5C and S5; STAR Methods). Most of the TFs for selected key regulons have been shown to be crucial for embryonic development (Table S4). For instance, GATA6 has demonstrated significance in the ICM of mouse, bovine, and human embryos.[35,36] Similarly, CDX2, GATA2, and GATA3 have been implicated in the TE of mouse, bovine, and human embryos.[19,35,37–40] Interestingly, for the pre-EGA stage, PRDM5 was identified as a key regulon, reflecting the arrested characteristics of these cells, as this TF is involved in G2/M arrest and apoptosis by suppressing the expression of several oncogenes and antagonizing WNT/β-catenin signaling.[41,42] These findings shed light on the combinations of TFs that underlie cell state transitions and cellular identity during bovine preimplantation embryogenesis.

Whole-genome abnormalities induce stress responses during embryonic genome activation

Although WG abnormalities did not result in obvious deviations in the preimplantation developmental program, we hypothesized that the imbalanced parental genome compositions in cells with WG abnormalities could lead to parent-specific gene expression patterns for genes predominantly expressed from only one parent's genome. Furthermore, these WG abnormalities may function as stress stimuli, inducing global transcriptomic changes that ultimately impair the overall developmental potential of cells. To investigate the parental genome-specific effects on gene expression, we compared the gene expression profiles of gynogenetic, androgenetic, and polyploid (diandric triploid and triandric tetraploid) cells to those of biparental diploid cells within each molecular developmental stage. Additionally, to capture the overall effects of WG abnormalities on gene expression, we aggregated all cells with WG abnormalities for combined analyses.

Differentially expressed (DE) genes were identified from the onset of EGA (Figure 6A), suggesting that WG abnormalities lead to gene expression changes during EGA. Only one DE gene was identified at the early blastocyst stage, indicating a high degree of similarity between normal cells and cells with WG abnormalities just before the first lineage specification. DE genes found in the combined analysis partially overlap with those identified in separate analyses (Figure S6; Table S5). Manual functional annotation revealed some parental genome specific effects. We noted the downregulation of the maternally imprinted gene *SNRPN* in gynogenetic cells during major EGA, aligning with its known paternal-specific expression.[43] Furthermore, we identified the upregulation of genes involved in cell adhesion (e.g., *RAPH1, PCDH17*) in polyploid cells during major EGA and at the TE stage (Figure 6B; Table S5). This indicates active cell adhesion-related processes, such as compaction in these cells, possibly caused by the additional paternal genome contribution.

Other DE genes observed in uniparental/polyploid cells, as well as those identified through combined analysis, were mainly involved in similar biological processes, indicating general cellular effects of WG abnormalities (Figure 6C; Table S5). We observed upregulation of cell-cycle/mitosis-related genes (e.g., *STIL*, *CCNYL1*), indicating active preparation for cell-cycle progression in cells with WG abnormalities. Meanwhile, we noted a downregulation of ribosomal protein genes (e.g., *RPL14*) and translation initiation factor genes (e.g., *EIF2S3*). It is known that during cellular adaptation to stress stimuli, growth-related genes, including those involved in ribosomes and translation,

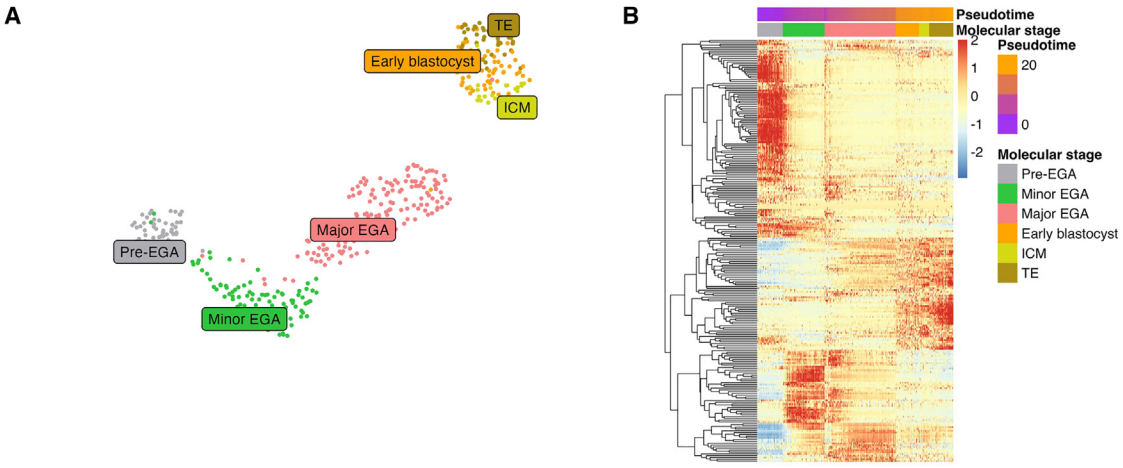

C

Molecular stage	Selected key regulons
Pre-EGA	SIX3, PRDM5, ZBTB43, SMC3, EBF1, HES7
Minor EGA	KLF17, MAX, ZNF143, THAP11, CHD1, IRF3
Major EGA	MITF, ARNT, RARB, HSF1, USF1, BRCA1
Early blastocyst	GATA2, TBX3
ICM	SOX15, NELFB, SREBF1, GATA6, ERF, MAZ
TE	CDX2, TCF7L1, JDP2, JUN, GATA2, GATA3

Figure 5. Distinct preimplantation cellular states are governed by specific key transcription factors

(A) UMAP displaying cell clustering based on regulon activity, with cells colored according to their macular developmental stage as depicted in Figure 4C.

(B) Heatmap of regulon activity. Each row represents one regulon, and each column represents one cell. The plot is generated using rescaled area under the curve (AUC) values, with cells ordered according to their molecular developmental stage and pseudotime values.

(C) Key regulons selected for each stage. See also Figure S5 and Table S4.

are typically repressed, prioritizing resources toward stress protection over rapid proliferation.[44] Our observation indicates reduced growth in cells with WG abnormalities as a consequence of the stress response triggered by WG abnormalities. Interestingly, for certain biological processes, DE genes were identified during EGA, leading to either upregulation or downregulation of these processes. No relevant DE genes were found for the early blastocyst stage, whereas in the TE, no DE genes or only DE genes resulting in upregulated activities of these processes were observed. The biological processes involved include apoptosis, cell death, stress response, DNA damage response, transcription regulation, metabolism, single transduction, cytoskeleton organization, and transport (Figure 6C; Table S5). This finding indicates that cells with WG abnormalities adapt to stimuli caused by genome imbalance through transcriptional responses during EGA, involving transient upregulation or downregulation of relevant genes.[44] A quiescent period follows during the early blastocyst stage, whereas the upregulation of specific genes in TE reflects the establishment of new steady-state levels. Additionally, we conducted differential regulon analysis, and DE regulons were identified for cells with WG abnormalities exclusively during EGA (Table S5). Most DE regulons are essential for embryonic development, and their bidirectional changes mirror the bidirectional gene expression alterations observed in differential gene expression analysis (Table S5), reflecting stress responses to WG abnormalities at the transcriptional factor level. For example, *SMAD3*, which was upregulated in WG abnormal cells, plays a pivotal role in mediating transforming growth factor β (TGF-β) signaling, a key pathway that regulates early developmental processes.[45] Similarly, *MYB*, also upregulated, influences over 80 cellular targets involved in development, cell survival, proliferation, and homeostasis.[46] Interestingly, two TFs among the DE regulons are associated with imprinting. One is the maternally imprinted *PLAG1*,[47] which, as expected, was upregulated in androgenetic cells. The other is *ZFP42*, which was downregulated in all WG abnormal cells. Since *ZFP42* plays a critical role in shielding imprinted domains from DNA methylation,[48] its downregulation suggests a potential impairment in the maintenance of imprinting induced by WG abnormalities.

In summary, we observed parental genome-specific effects induced by WG abnormalities, suggesting distinct roles of the maternal and paternal genomes. Moreover, we identified universal cellular responses to WG abnormalities, marked by active

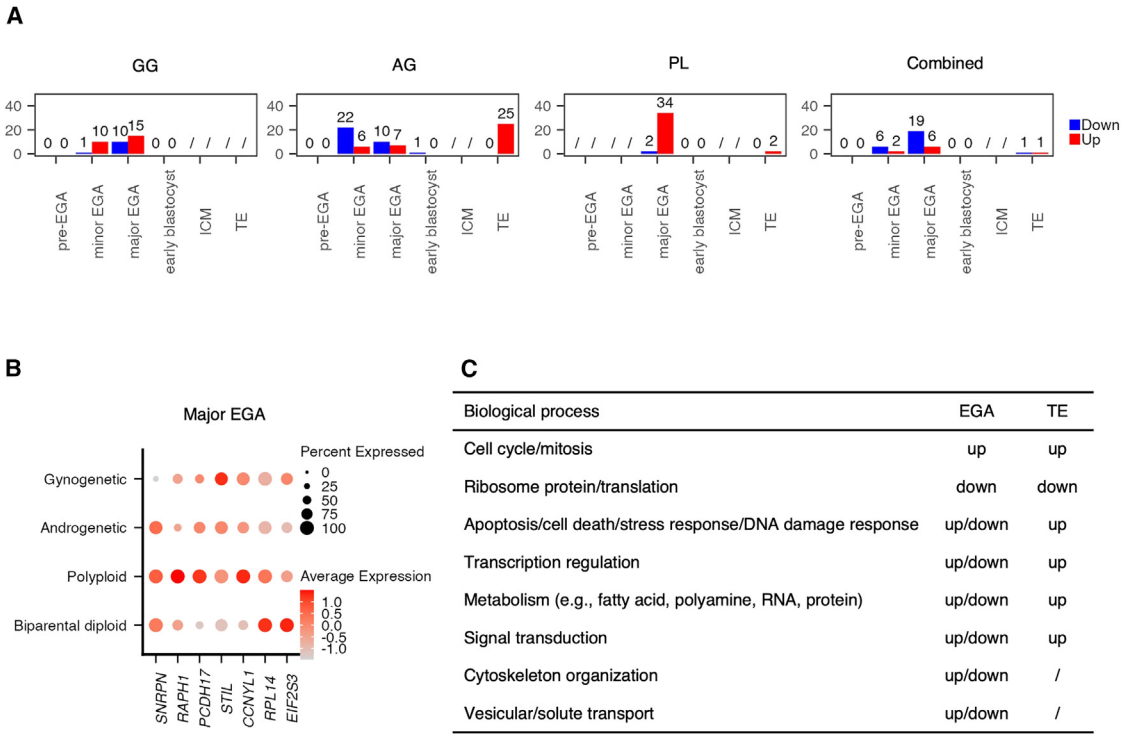

C

Biological process	EGA	TE
Cell cycle/mitosis	up	up
Ribosome protein/translation	down	down
Apoptosis/cell death/stress response/DNA damage response	up/down	up
Transcription regulation	up/down	up
Metabolism (e.g., fatty acid, polyamine, RNA, protein)	up/down	up
Signal transduction	up/down	up
Cytoskeleton organization	up/down	/
Vesicular/solute transport	up/down	/

Figure 6. Whole-genome abnormalities induce stress responses during embryonic genome activation

(A) Numbers of DE genes identified in gynogenetic (GG), androgenetic (AG), polyploid (PL), and combined WG-aberrant cells compared to biparental diploid cells for each stage. The "/" symbol denotes comparisons not conducted due to insufficient cells.

(B) Gene expression dot plot for DE genes during major EGA.

(C) Overall alterations in biological processes reflected by deviations in gene expression. "/" if no DE genes observed. See also Figures S3 and S6 and Table S5.

preparation for cell-cycle progression alongside reduced cell growth. Bidirectional alterations in specific biological processes and regulons during EGA, and their eventual balance, may dictate whether cells arrest or advance toward the blastocyst stage. Overall, these observed stress responses provide insights into the impaired development caused by WG abnormalities.

DISCUSSION

WG abnormalities are a type of chromosomal error frequently observed in spontaneous abortions[3] and on very rare occasions in a chimeric state in live-born individuals.[8] Contrary to its implications in abnormal pregnancy and congenital abnormalities, the proposed origins of such anomalies are deductions from surviving cells at later stages or remain speculative, and their effect on early development remains largely unknown. Here, we provide fundamental insights into the emergence and early developmental biology of gynogenetic, androgenetic, and polyploid blastomeres using haplotyping and single-cell transcriptome analysis. We demonstrated the occurrence of uniparental and polyploid blastomeres through a non-canonical division during the first zygotic cleavage, which segregates parental genomes into distinct blastomeres. We not only confirmed our previous observation[15] that heterogoneic division mostly coincides with multipolar first cleavage in polyspermic embryos but also identified, for the first time, heterogoneic division occurring with bipolar first cleavage in normally fertilized embryos. The reduced developmental potential of uniparental and polyploid blastomeres derived from heterogoneic division was evidenced by a lower blastocyst rate and a delay in pseudotime values beginning from T2, coinciding with major EGA. Stress responses observed during EGA suggest the cells' efforts to combat fitness challenges induced by aberrant genome composition, with the outcome determining whether they arrest or progress further to the blastocyst stage.

For the embryo undergoing bipolar first cleavage but exhibiting heterogoneic division, one of the two daughter blastomeres was identified as androgenetic, whereas the other was gynogenetic based on the haplotyping results. The presence of the same paternal haplotype across the genome indicates monospermic fertilization. Consequently, it is reasonable to infer that the paternal and maternal genomes segregated into distinct blastomeres due to the failure of separate parental zygotic spindles to align, a hypothesis supported by previous studies. First, Schneider et al. observed the assembly of dual spindles in bovine zygotes.[49] In cases where the alignment of the two spindles was perturbed, the parental genomes could segregate in different directions, leading to gross mitotic aberrations. Second, we previously identified heterogoneic division in a monospermic bovine zygote with a tripolar first cleavage. Live-imaging experiments with bovine zygotes expressing transient microtubule and chromatin markers revealed that the parental genomes failed to congress and instead

formed two separate parental spindles perpendicular to each other. After cleavage, this resulted in a mononucleated monoparental blastomere, a multinucleated biparental blastomere containing an additional copy of chromosomes from one parent, and an anuclear blastomere, illustrating how failed congression of parental genomes can lead to heterogoneic division.[15] Taken together, these previous findings suggest that the failure of the two parental zygotic spindles to align, followed by their segregation into distinct blastomeres, can result in heterogoneic division. This mechanism could explain how a monospermic embryo with a bipolar first cleavage gave rise to an androgenetic and a gynogenetic blastomere in the present study.

Stress responses observed during EGA reflect the general cellular effects induced by WG abnormalities, which inhibit protein synthesis, as evidenced by the reduced expression of translation initiation factors and ribosomal proteins in WG abnormal cells. Genomic-instability-induced downregulation of translation initiation factors has been reported.[50] Additionally, imbalanced expression of ribosomal proteins in stressed cells has been observed, acting as a stress sensor that triggers p53 activation by suppressing the activity of the MDM2 E3 ubiquitin ligase,[51] indicating that p53-centered stress responses are likely at play in WG abnormal cells. Ploidy errors themselves have also been linked to the activation of the p53 response.[52] As a transcription factor, p53 regulates target genes involved in various processes, including apoptosis, cell-cycle arrest, cellular senescence, DNA repair, and metabolic adaptation.[53] These diverse responses align well with the bidirectional gene expression changes involving various biological processes observed in this study, suggesting that different levels of genome abnormalities lead to distinct outcomes depending on the cellular response. Severely affected cells are likely to undergo p53-dependent cellular senescence or apoptosis, whereas mildly affected ones may experience p53-dependent growth arrest and DNA repair. Interestingly, in cells with WG abnormalities, we observed upregulation of cell-cycle/mitosis-related genes involved in centriole duplication, kinetochore protein assembly, chromosome alignment and segregation, and cytokinesis. This indicates active preparation for cell-cycle progression, which seems counterintuitive in light of the abnormal karyotype and the cell-cycle arrest typically induced by p53 target genes. A plausible explanation is that most WG abnormal cells actively prepare for cell-cycle progression in order to survive despite the genomic errors. This is similar to the overexpression of cell-cycle drivers observed in cleavage-stage human embryos, which are known to exhibit high chromosomal instability.[54] Although a fraction of cells with severely affected genomes undergo mitotic arrest, the overall effect is compensated for by the abundant expression of cell-cycle drivers in other cells. Interestingly, a previous analysis by Santaguida et al. supports this idea, showing that the majority of cells with mis-segregated chromosomes continued to proliferate, whereas a small proportion of cells with highly complex karyotypes and signs of DNA damage are arrested in G1 following p53 activation.[55]

Other studies have examined the preimplantation development of mammalian uniparental embryos. These embryos were generated through various methods, including nuclear manipulation,[34,56,57] *in vitro* induction[34,58–61] or natural occurrence[62] of parthenogenetic development in unfertilized oocytes, as well as bisection of one-cell fertilized eggs.[63] Similar to this study, they have shown a decrease in the morula/blastocyst rate compared to biparental diploid embryos, alongside poorer morphology and reduced cell count in resulting blastocysts.[34,62] Several studies have also affirmed the compatibility of diploid uniparental genome constitution with later development.[56,59] Moreover, diploid gynogenetic cells have been identified in various organs of live-born chimeric mice developed from aggregated chimeric embryos.[60] These findings are consistent with observations in humans, suggesting that uniparental cell lines are typically selected against during development but can persist until late pregnancy and even be compatible with live birth. This study demonstrates that heterogoneic division could serve as an origin of uniparental and polyploid cell lines observed during late development.

We identified anuclear cells at different stages, which is in agreement with previous observations in bovine,[15,64] rhesus,[16] and human[65] embryos. Most anuclear blastomeres were identified following multipolar first cleavage, suggesting a link between this cleavage pattern and the origin of anuclear cells. Additionally, we observed that some anuclear cells can undergo cleavage without nuclei. However, the molecular mechanisms driving anuclear blastomere formation and spontaneous cleavage remain poorly understood. For instance, Hardy et al. suggested that nuclear fragmentation could lead to anucleate cells through degradation and that asymmetric cytokinesis might result in anucleate blastomeres.[65] Additionally, Baruni et al. observed in *Caenorhabditis elegans* embryos that anucleate, centrosome-containing cells can proceed with cytokinetic furrowing,[66] pointing to a potential role for the centrosome in anuclear cell cleavage. Furthermore, while cytoplasmic division typically relies on nuclear division and mitotic signals, Bakshi et al. recently demonstrated in *Drosophila* embryos that cytoplasm can compartmentalize and, in rare cases, divide repeatedly without nuclei or mitotic CDK/cyclin complexes, a phenomenon relevant to mitotically delayed nuclei.[67] We hypothesize that a similar mechanism may operate in mammalian embryos, explaining both the formation and cleavage of anuclear blastomeres observed here, with anuclear cells arising from mother cells containing nuclei with delayed mitosis. These findings collectively underscore the need for further investigation into the detailed mechanisms underlying the presence of anuclear cells in mammalian embryos and their potential roles in embryo development.

Insights from this study raise clinical concerns. First, in IVF laboratories, human embryos with two pronuclei (PN) are preferentially selected for transfer.[68] We demonstrate here that zygotes with three PN may result in a mixture of biparental diploid and uniparental/polyploid blastomeres. Since the latter are developmentally compromised, the resulting embryo may still develop normally. Second, there is a growing trend in many laboratories to monitor embryonic development using time-lapse microscopy and rank embryos based on cleavage kinetics.[68–71] Embryos with multipolar first cleavage are typically given a low rank. We showed here that 22% of embryos with a multipolar first cleavage exhibited normal, equal division of the genome with additional anuclear cells. It would be unjust to lower rank these embryos since they have the potential to lead to healthy babies.

Additionally, even though uniparental/polyploid cells are normally generated with multipolar first cleavage, it is not uncommon that biparental diploid blastomeres are generated together, which may gain developmental advantage and lead to normal development. Third, embryos typically ranked high, characterized by a normal pronuclei count and bipolar first cleavage, may still experience WG segregation errors, leading to the generation of solely uniparental cells, posing a potential risk of abnormal pregnancy. Rather than removing or keeping embryos based on apparent abnormalities, it might be better to evaluate the genome constitution of preimplantation embryos and deselect those with WG abnormalities, while retaining those with a normal chromosome count and parental haplotype constitution. Preimplantation genetic testing for aneuploidy (PGT-A) has become a common practice to select embryos with a normal number of chromosomes for transfer. However, the majority of PGT-A tests only measure aneuploidies, with only some measuring the parental haplotype constitution.[72] We suggest the use of genotyping/haplotyping together with PGT-A[23,24] to check both chromosome count and parental haplotype constitution and select against WG abnormalities. This approach is likely to further improve the overall IVF success rate.[73]

In conclusion, this study provides insights into the origin and early development of uniparental/polyploid blastomeres. We demonstrated their overall impaired developmental potential, primarily due to stress responses triggered by WG abnormalities during EGA. Blastomeres that successfully navigate through this phase and progress to the blastocyst stage may constitute a significant fraction of embryos and contribute to abnormal development. Our findings underscore the importance of routine screening against embryos bearing WG abnormalities in IVF labs.

Limitations of the study

There are several limitations to our study. First, the classification of the first cleavage as bipolar or multipolar was based on cell numbers observed at predefined timing post-fertilization (optimal timing derived from a pilot study) rather than direct observation of the division process. It is known that a daughter cell in a two-cell stage embryo can rapidly undergo a second division, producing a three-cell embryo.[74] Our embryo classification method, therefore, risks misclassifying bipolar-cleaved embryos with rapid second cleavage as multipolar. This limitation could be overcome by incorporating time-lapse monitoring in future studies. Second, although previous studies have shown that the first cleavage is especially error prone,[25] with dual spindle assembly increasing the likelihood of WG segregation errors,[49] and that WG segregation errors are primarily observed during this stage,[16] culturing individual blastomeres may still introduce WG abnormalities. Third, the *in vitro* procedures applied in our study, including oocyte maturation, fertilization, and blastomere culture, have been shown to increase genomic instability in embryos.[9,75]

RESOURCE AVAILABILITY

Lead contact

Further information and requests for resources and reagents should be directed to and will be fulfilled by the lead contact, Joris Robert Vermeesch (Joris.Vermeesch@KULeuven.be).

Materials availability

This study did not generate new unique reagents.

Data and code availability

- Data: the GBS and single-cell RNA sequencing data reported in this paper are available at the European Nucleotide Archive (ENA) under project number PRJEB76932 (https://www.ebi.ac.uk/ena/browser/view/PRJEB76932).
- Code: this paper does not report original code.
- Additional information: any additional information required to reanalyze the data reported in this paper is available from the lead contact upon request.

ACKNOWLEDGMENTS

Funding was received from the Marie Skłodowska-Curie grant agreement No 813707 (MATER) and from the KU Leuven, C1-C14/22/125 to J.R.V. and T.V. T.L. and T.V. were supported by the Research Foundation Flanders (FWO: G0C6120N, G088621N and I001818N). Y.Z. was supported by the Marie Skłodowska-Curie grant agreement No 813707 (MATER). A.F. is supported by the European Union's Horizon 2020 research and innovation program under the Marie Skłodowska-Curie grant agreement No 860960 and BOF22/ITN/036.

AUTHOR CONTRIBUTIONS

J.R.V., A.V.S., and K.S. conceptualized and designed the study. A.F. conducted embryo experiments, with assistance from T.D.C. and D.A.V. T.L. and T.V. performed G&T-seq. G.P. and T.J. conducted GBS processing and coordinated sequencing. Y.Z. conducted bioinformatics analysis. Y.Z., J.R.V., and O.T. interpreted the data. Y.Z., J.R.V., A.F., and A.K. wrote the manuscript. All co-authors reviewed and approved the manuscript.

DECLARATION OF INTERESTS

T.V. and J.R.V. are co-inventors on licensed patents WO/2011/157846 (Methods for haplotyping single cells), WO/2014/053664 (High-throughput genotyping by sequencing low amounts of genetic material), and WO/2015/028576 (Haplotyping and copy number typing using polymorphic variant allelic frequencies).

STAR★METHODS

Detailed methods are provided in the online version of this paper and include the following:

- KEY RESOURCES TABLE
- EXPERIMENTAL MODEL AND STUDY PARTICIPANT DETAILS
- METHOD DETAILS
  - Single-cell collection from bovine blastomere outgrowths
  - DNA and RNA separation, library preparation and sequencing
  - Data analysis
- QUANTIFICATION AND STATISTICAL ANALYSIS

SUPPLEMENTAL INFORMATION

Supplemental information can be found online at https://doi.org/10.1016/j.isci.2025.112337.

Received: September 20, 2024
Revised: December 3, 2024
Accepted: March 28, 2025
Published: April 2, 2025

REFERENCES

1. Hassold, T., and Hunt, P. (2001). To err (meiotically) is human: the genesis of human aneuploidy. Nat. Rev. Genet. *2*, 280–291. https://doi.org/10.1038/35066065.
2. Vanneste, E., Voet, T., Le Caignec, C., Ampe, M., Konings, P., Melotte, C., Debrock, S., Amyere, M., Vikkula, M., Schuit, F., et al. (2009). Chromosome instability is common in human cleavage-stage embryos. Nat. Med. *15*, 577–583. https://doi.org/10.1038/nm.1924.
3. Hassold, T., Chen, N., Funkhouser, J., Jooss, T., Manuel, B., Matsuura, J., Matsuyama, A., Wilson, C., Yamane, J.A., and Jacobs, P.A. (1980). A cytogenetic study of 1000 spontaneous abortions. Ann. Hum. Genet. *44*, 151–178. https://doi.org/10.1111/J.1469-1809.1980.TB00955.X.
4. Masset, H., Tšuiko, O., and Vermeesch, J.R. (2021). Genome-wide abnormalities in embryos: Origins and clinical consequences. Prenat. Diagn. *41*, 554–563. https://doi.org/10.1002/PD.5895.
5. Zaragoza, M.V., Surti, U., Redline, R.W., Millie, E., Chakravarti, A., and Hassold, T.J. (2000). Parental origin and phenotype of triploidy in spontaneous abortions: Predominance of diandry and association with the partial hydatidiform mole. Am. J. Hum. Genet. *66*, 1807–1820. https://doi.org/10.1086/302951.
6. Sherard, J., Bean, C., Bove, B., DelDuca, V., Esterly, K.L., Karcsh, H.J., Munshi, G., Reamer, J.F., Suazo, G., and Wilmoth, D. (1986). Long survival in a 69,XXY triploid male. Am. J. Med. Genet. *25*, 307–312. https://doi.org/10.1002/AJMG.1320250216.
7. Seckl, M.J., Sebire, N.J., and Berkowitz, R.S. (2010). Gestational trophoblastic disease. Lancet *376*, 717–729. https://doi.org/10.1016/S0140-6736(10)60280-2.
8. Madan, K. (2020). Natural human chimeras: A review. Eur. J. Med. Genet. *63*, 103971. https://doi.org/10.1016/J.EJMG.2020.103971.
9. Tšuiko, O., Catteeuw, M., Zamani Esteki, M., Destouni, A., Bogado Pascottini, O., Besenfelder, U., Havlicek, V., Smits, K., Kurg, A., Salumets, A., et al. (2017). Genome stability of bovine *in vivo*-conceived cleavage-stage embryos is higher compared to *in vitro*-produced embryos. Hum. Reprod. *32*, 2348–2357. https://doi.org/10.1093/HUMREP/DEX286.
10. Hansen, P.J. (2010). Medawar redux - an overview on the use of farm animal models to elucidate principles of reproductive immunology. Am. J. Reprod. Immunol. *64*, 225–230. https://doi.org/10.1111/J.1600-0897.2010.00900.X.
11. Santos, R.R., Schoevers, E.J., and Roelen, B.A.J. (2014). Usefulness of bovine and porcine IVM/IVF models for reproductive toxicology. Reprod. Biol. Endocrinol. *12*, 117. https://doi.org/10.1186/1477-7827-12-117.
12. Dunn, H.O., McEntee, K., and Hansel, W. (1970). Diploid-triploid chimerism in a bovine true hermaphrodite. Cytogenetics (Basel) *9*, 245–259. https://doi.org/10.1159/000130095.
13. Destouni, A., Zamani Esteki, M., Catteeuw, M., Tšuiko, O., Dimitriadou, E., Smits, K., Kurg, A., Salumets, A., Van Soom, A., Voet, T., and Vermeesch, J.R. (2016). Zygotes segregate entire parental genomes in distinct blastomere lineages causing cleavage-stage chimerism and mixoploidy. Genome Res. *26*, 567–578. https://doi.org/10.1101/GR.200527.115.
14. Meinecke, B., Kuiper, H., Drögemüller, C., Leeb, T., and Meinecke-Tillmann, S. (2003). A Mola Hydatidosa Coexistent with a Foetus in a Bovine Freemartin Pregnancy. Placenta *24*, 107–112. https://doi.org/10.1053/PLAC.2002.0872.
15. De Coster, T., Masset, H., Tšuiko, O., Catteeuw, M., Zhao, Y., Dierckxsens, N., Aparicio, A.L., Dimitriadou, E., Debrock, S., Peeraer, K., et al. (2022). Parental genomes segregate into distinct blastomeres during multipolar zygotic divisions leading to mixoploid and chimeric blastocysts. Genome Biol. *23*, 1–29. https://doi.org/10.1186/S13059-022-02763-2.
16. Daughtry, B.L., Rosenkrantz, J.L., Lazar, N.H., Fei, S.S., Redmayne, N., Torkenczy, K.A., Adey, A., Yan, M., Gao, L., Park, B., et al. (2019). Single-cell sequencing of primate preimplantation embryos reveals chromosome elimination via cellular fragmentation and blastomere exclusion. Genome Res. *29*, 367–382. https://doi.org/10.1101/GR.239830.118.
17. Ottolini, C.S., Kitchen, J., Xanthopoulou, L., Gordon, T., Summers, M.C., and Handyside, A.H. (2017). Tripolar mitosis and partitioning of the genome arrests human preimplantation development *in vitro*. Sci. Rep. *7*, 9744–9810. https://doi.org/10.1038/s41598-017-09693-1.
18. Fragouli, E., Alfarawati, S., Spath, K., Jaroudi, S., Sarasa, J., Enciso, M., and Wells, D. (2013). The origin and impact of embryonic aneuploidy. Hum. Genet. *132*, 1001–1013. https://doi.org/10.1007/S00439-013-1309-0.
19. Gallardo, E.F., Sifrim, A., Chappell, J., Demeulemeester, J., Herrmann, J.C., Vermotte, R., Kerremans, A., Van Der Haegen, M., Herck, J.V., Vanuytven, S., et al. (2023). A multi-omics genome-and-transcriptome single-cell atlas of human preimplantation embryogenesis reveals the cellular and molecular impact of chromosome instability. Preprint at bioRxiv. https://doi.org/10.1101/2023.03.08.530586.
20. Tšuiko, O., Vanneste, M., Melotte, C., Ding, J., Debrock, S., Masset, H., Peters, M., Salumets, A., De Leener, A., Pirard, C., et al. (2021). Haplotyping-based preimplantation genetic testing reveals parent-of-origin specific mechanisms of aneuploidy formation. NPJ Genom. Med. *6*, 81. https://doi.org/10.1038/S41525-021-00246-0.
21. Johnson, W.H., Loskutoff, N.M., Plante, Y., and Betteridge, K.J. (1995). Production of four identical calves by the separation of blastomeres from an *in vitro* derived four-cell embryo. Vet. Rec. *137*, 15–16. https://doi.org/10.1136/VR.137.1.15.
22. Willadsen, S.M. (1980). The viability of early cleavage stages containing half the normal number of blastomeres in the sheep. Reproduction *59*, 357–362. https://doi.org/10.1530/JRF.0.0590357.
23. Masset, H., Ding, J., Dimitriadou, E., Debrock, S., Tšuiko, O., Smits, K., Peeraer, K., Voet, T., Zamani Esteki, M., and Vermeesch, J.R. (2022). Single-cell genome-wide concurrent haplotyping and copy-number profiling through genotyping-by-sequencing. Nucleic Acids Res. *50*, e63. https://doi.org/10.1093/NAR/GKAC134.
24. Zamani Esteki, M., Dimitriadou, E., Mateiu, L., Melotte, C., Van der Aa, N., Kumar, P., Das, R., Theunis, K., Cheng, J., Legius, E., et al. (2015). Concurrent Whole-Genome Haplotyping and Copy-Number Profiling of Single Cells. Am. J. Hum. Genet. *96*, 894–912. https://doi.org/10.1016/J.AJHG.2015.04.011.
25. Currie, C.E., Ford, E., Benham Whyte, L., Taylor, D.M., Mihalas, B.P., Erent, M., Marston, A.L., Hartshorne, G.M., and McAinsh, A.D. (2022). The first mitotic division of human embryos is highly error prone. Nat. Commun. *13*, 6755. https://doi.org/10.1038/s41467-022-34294-6.
26. Kola, I., Trounson, A., Dawson, G., and Rogers, P. (1987). Tripronuclear human oocytes: altered cleavage patterns and subsequent karyotypic analysis of embryos. Biol. Reprod. *37*, 395–401. https://doi.org/10.1095/BIOLREPROD37.2.395.
27. Zhan, Q., Ye, Z., Clarke, R., Rosenwaks, Z., and Zaninovic, N. (2016). Direct Unequal Cleavages: Embryo Developmental Competence, Genetic Constitution and Clinical Outcome. PLoS One *11*, e0166398. https://doi.org/10.1371/JOURNAL.PONE.0166398.
28. Chatzimeletiou, K., Morrison, E.E., Prapas, N., Prapas, Y., and Handyside, A.H. (2005). Spindle abnormalities in normally developing and arrested human preimplantation embryos *in vitro* identified by confocal laser scanning microscopy. Hum. Reprod. *20*, 672–682. https://doi.org/10.1093/HUMREP/DEH652.
29. Sembon, S., Iwamoto, M., Hashimoto, M., Oishi, T., Fuchimoto, D., Suzuki, S., Yazaki, S., and Onishi, A. (2012). Porcine androgenetic embryos develop to fetal stage in recipient mothers. Theriogenology *78*, 225–231. https://doi.org/10.1016/J.THERIOGENOLOGY.2012.01.021.
30. Latham, K.E., Akutsu, H., Patel, B., and Yanagimachi, R. (2002). Comparison of gene expression during preimplantation development between diploid and haploid mouse embryos. Biol. Reprod. *67*, 386–392. https://doi.org/10.1095/BIOLREPROD67.2.386.

31. Ma, L.B., Yang, L., Zhang, Y., Cao, J.W., Hua, S., and Li, J.X. (2008). Quantitative analysis of mitochondrial RNA in goat–sheep cloned embryos. Mol. Reprod. Dev. *75*, 33–39. https://doi.org/10.1002/MRD.20736.

32. May-Panloup, P., Vignon, X., Chrétien, M.F., Heyman, Y., Tamassia, M., Mathièry, Y., and Reynier, P. (2005). Increase of mitochondrial DNA content and transcripts in early bovine embryogenesis associated with upregulation of mtTFA and NRF1 transcription factors. Reprod. Biol. Endocrinol. *3*, 1–8. https://doi.org/10.1186/1477-7827-3-65.

33. Thundathil, J., Filion, F., and Smith, L.C. (2005). Molecular control of mitochondrial function in preimplantation mouse embryos. Mol. Reprod. Dev. *71*, 405–413. https://doi.org/10.1002/MRD.20260.

34. Leng, L., Sun, J., Huang, J., Gong, F., Yang, L., Zhang, S., Yuan, X., Fang, F., Xu, X., Luo, Y., et al. (2019). Single-Cell Transcriptome Analysis of Uniparental Embryos Reveals Parent-of-Origin Effects on Human Preimplantation Development. Cell Stem Cell *25*, 697–712.e6. https://doi.org/10.1016/j.stem.2019.09.004.

35. Niakan, K.K., and Eggan, K. (2013). Analysis of human embryos from zygote to blastocyst reveals distinct gene expression patterns relative to the mouse. Dev. Biol. *375*, 54–64. https://doi.org/10.1016/J.YDBIO.2012.12.008.

36. Marsico, T.V., Valente, R.S., Annes, K., Oliveira, A.M., Silva, M.V., and Sudano, M.J. (2023). Species-specific molecular differentiation of embryonic inner cell mass and trophectoderm: A systematic review. Anim. Reprod. Sci. *252*, 107229. https://doi.org/10.1016/J.ANIREPROSCI.2023.107229.

37. Home, P., Kumar, R.P., Ganguly, A., Saha, B., Milano-Foster, J., Bhattacharya, B., Ray, S., Gunewardena, S., Paul, A., Camper, S.A., et al. (2017). Genetic redundancy of GATA factors in the extraembryonic trophoblast lineage ensures the progression of preimplantation and postimplantation mammalian development. Development *144*, 876–888. https://doi.org/10.1242/DEV.145318.

38. Gerri, C., McCarthy, A., Alanis-Lobato, G., Demtschenko, A., Bruneau, A., Loubersac, S., Fogarty, N.M.E., Hampshire, D., Elder, K., Snell, P., et al. (2020). Initiation of a conserved trophectoderm program in human, cow and mouse embryos. Nature *587*, 443–447. https://doi.org/10.1038/s41586-020-2759-x.

39. Nagatomo, H., Kagawa, S., Kishi, Y., Takuma, T., Sada, A., Yamanaka, K.I., Abe, Y., Wada, Y., Takahashi, M., Kono, T., and Kawahara, M. (2013). Transcriptional Wiring for Establishing Cell Lineage Specification at the Blastocyst Stage in Cattle1. Biol. Reprod. *88*, 158–159. https://doi.org/10.1095/BIOLREPROD.113.108993/2514370.

40. Negrón-Pérez, V.M., Zhang, Y., and Hansen, P.J. (2017). Single-cell gene expression of the bovine blastocyst. Reproduction *154*, 627–644. https://doi.org/10.1530/REP-17-0345.

41. Deng, Q., and Huang, S. (2004). PRDM5 is silenced in human cancers and has growth suppressive activities. Oncogene *23*, 4903–4910. https://doi.org/10.1038/sj.onc.1207615.

42. Shu, X.S., Geng, H., Li, L., Ying, J., Ma, C., Wang, Y., Poon, F.F., Wang, X., Ying, Y., Yeo, W., et al. (2011). The Epigenetic Modifier PRDM5 Functions as a Tumor Suppressor through Modulating WNT/β-Catenin Signaling and Is Frequently Silenced in Multiple Tumors. PLoS One *6*, e27346. https://doi.org/10.1371/JOURNAL.PONE.0027346.

43. Lucifero, D., Suzuki, J., Bordignon, V., Martel, J., Vigneault, C., Therrien, J., Filion, F., Smith, L.C., and Trasler, J.M. (2006). Bovine SNRPN Methylation Imprint in Oocytes and Day 17 In Vitro-Produced and Somatic Cell Nuclear Transfer Embryos. Biol. Reprod. *75*, 531–538. https://doi.org/10.1095/BIOLREPROD.106.051722.

44. López-Maury, L., Marguerat, S., and Bähler, J. (2008). Tuning gene expression to changing environments: from rapid responses to evolutionary adaptation. Nat. Rev. Genet. *9*, 583–593. https://doi.org/10.1038/nrg2398.

45. Liu, L., Liu, X., Ren, X., Tian, Y., Chen, Z., Xu, X., Du, Y., Jiang, C., Fang, Y., Liu, Z., et al. (2016). Smad2 and Smad3 have differential sensitivity in relaying TGFβ signaling and inversely regulate early lineage specification. Sci. Rep. *6*, 21602. https://doi.org/10.1038/srep21602.

46. Ramsay, R.G., and Gonda, T.J. (2008). MYB function in normal and cancer cells. Nat. Rev. Cancer *8*, 523–534. https://doi.org/10.1038/nrc2439.

47. D'Occhio, M.J., Campanile, G., Baruselli, P.S., Porto Neto, L.R., Hayes, B.J., Snr, A.C., and Fortes, M.R.S. (2024). Pleomorphic adenoma gene1 in reproduction and implication for embryonic survival in cattle: a review. J. Anim. Sci. *102*, skae103. https://doi.org/10.1093/JAS/SKAE103.

48. Kim, J.D., Kim, H., Ekram, M.B., Yu, S., Faulk, C., and Kim, J. (2011). Rex1/Zfp42 as an epigenetic regulator for genomic imprinting. Hum. Mol. Genet. *20*, 1353–1362. https://doi.org/10.1093/HMG/DDR017.

49. Schneider, I., de Ruijter-Villani, M., Julius Hossain, M., Stout, T.A.E., and Ellenberg, J. (2021). Dual spindles assemble in bovine zygotes despite the presence of paternal centrosomes. J. Cell Biol. *220*, e202010106. https://doi.org/10.1083/JCB.202010106.

50. Sheikh, M.S., and Fornace, A.J. (1999). Regulation of translation initiation following stress. Oncogene *18*, 6121–6128. https://doi.org/10.1038/sj.onc.1203131.

51. Kim, T.-H., Leslie, P., Zhang, Y., Kim, T.-H., Leslie, P., and Zhang, Y. (2014). Ribosomal proteins as unrevealed caretakers for cellular stress and genomic instability. Oncotarget *5*, 860–871. https://doi.org/10.18632/ONCOTARGET.1784.

52. Aylon, Y., and Oren, M. (2011). p53: guardian of ploidy. Mol. Oncol. *5*, 315–323. https://doi.org/10.1016/J.MOLONC.2011.07.007.

53. Thomas, A.F., Kelly, G.L., and Strasser, A. (2022). Of the many cellular responses activated by TP53, which ones are critical for tumour suppression? Cell Death Differ. *29*, 961–971. https://doi.org/10.1038/s41418-022-00996-z.

54. Kiessling, A.A., Bletsa, R., Desmarais, B., Mara, C., Kallianidis, K., and Loutradis, D. (2010). Genome-wide microarray evidence that 8-Cell human blastomeres over-express cell cycle drivers and under-express checkpoints. J. Assist. Reprod. Genet. *27*, 265–276. https://doi.org/10.1007/S10815-010-9407-6.

55. Santaguida, S., Richardson, A., Iyer, D.R., M'Saad, O., Zasadil, L., Knouse, K.A., Wong, Y.L., Rhind, N., Desai, A., and Amon, A. (2017). Chromosome Mis-segregation Generates Cell-Cycle-Arrested Cells with Complex Karyotypes that Are Eliminated by the Immune System. Dev. Cell *41*, 638–651.e5. https://doi.org/10.1016/J.DEVCEL.2017.05.022.

56. Hoppe, P.C., and Illmensee, K. (1977). Microsurgically produced homozygous-diploid uniparental mice. Proc. Natl. Acad. Sci. USA *74*, 5657–5661. https://doi.org/10.1073/PNAS.74.12.5657.

57. Xu, J., Shu, Y., Yao, G., Zhang, Y., Niu, W., Zhang, Y., Ma, X., Jin, H., Zhang, F., Shi, S., et al. (2021). Parental methylome reprogramming in human uniparental blastocysts reveals germline memory transition. Genome Res. *31*, 1519–1530. https://doi.org/10.1101/GR.273318.120.

58. Hao, Y., Lai, L., Mao, J., Im, G.S., Bonk, A., and Prather, R.S. (2004). Apoptosis in Parthenogenetic Preimplantation Porcine Embryos. Biol. Reprod. *70*, 1644–1649. https://doi.org/10.1095/BIOLREPROD.103.026005.

59. Hwang, I.S., Park, M.R., Lee, H.S., Kwak, T.U., Son, H.Y., Kang, J.K., Lee, J.W., Lee, K., Park, E.W., and Hwang, S. (2020). Developmental and Degenerative Characterization of Porcine Parthenogenetic Fetuses during Early Pregnancy. Animals *10*, 622. https://doi.org/10.3390/ANI10040622.

60. Ito, M., Kaneko-Ishino, T., Ishino, F., Matsuhashi, M., Yokoyama, M., and Katsuki, M. (1991). Fate of haploid parthenogenetic cells in mouse chimeras during development. J. Exp. Zool. *257*, 178–183. https://doi.org/10.1002/JEZ.1402570206.

61. Liu, L., Trimarchi, J.R., and Keefe, D.L. (2002). Haploidy but Not Parthenogenetic Activation Leads to Increased Incidence of Apoptosis in Mouse Embryos. Biol. Reprod. *66*, 204–210. https://doi.org/10.1095/BIOLREPROD66.1.204.

62. Hardy, K., Handyside, A.H., and Winston, R.M. (1989). The human blastocyst: cell number, death and allocation during late preimplantation development *in vitro*. Development *107*, 597–604. https://doi.org/10.1242/DEV.107.3.597.

63. Tarkowski, A.K. (1977). In vitro development of haploid mouse embryos produced by bisection of one-cell fertilized eggs. Development *38*, 187–202. https://doi.org/10.1242/DEV.38.1.187.

64. Brooks, K.E., Daughtry, B.L., Davis, B., Yan, M.Y., Fei, S.S., Shepherd, S., Carbone, L., and Chavez, S.L. (2022). Molecular contribution to embryonic aneuploidy and karyotypic complexity in initial cleavage divisions ofmammalian development. Development *149*, dev198341. https://doi.org/10.1242/DEV.198341.

65. Hardy, K., Winston, R.M., and Handyside, A.H. (1993). Binucleate blastomeres in preimplantation human embryos *in vitro*: failure of cytokinesis during early cleavage. Reproduction *98*, 549–558. https://doi.org/10.1530/JRF.0.0980549.

66. Baruni, J.K., Munro, E.M., and von Dassow, G. (2008). Cytokinetic furrowing in toroidal, binucleate and anucleate cells in C. elegans embryos. J. Cell Sci. *121*, 306–316. https://doi.org/10.1242/JCS.022897.

67. Bakshi, A., Iturra, F.E., Alamban, A., Rosas-Salvans, M., Dumont, S., and Aydogan, M.G. (2023). Cytoplasmic division cycles without the nucleus and mitotic CDK/cyclin complexes. Cell *186*, 4694–4709.e16. https://doi.org/10.1016/J.CELL.2023.09.010.

68. Balaban, B., Brison, D., Calderón, G., Catt, J., Conaghan, J., Cowan, L., Ebner, T., Gardner, D., Hardarson, T., Lundin, K., et al. (2011). The Istanbul consensus workshop on embryo assessment: proceedings of an expert meeting. Hum. Reprod. *26*, 1270–1283. https://doi.org/10.1093/HUMREP/DER037.

69. Sugimura, S., Akai, T., and Imai, K. (2017). Selection of viable *in vitro*-fertilized bovine embryos using time-lapse monitoring in microwell culture dishes. J. Reprod. Dev. *63*, 353–357. https://doi.org/10.1262/JRD.2017-041.

70. Sugimura, S., Akai, T., Hashiyada, Y., Somfai, T., Inaba, Y., Hirayama, M., Yamanouchi, T., Matsuda, H., Kobayashi, S., Aikawa, Y., et al. (2012). Promising System for Selecting Healthy In Vitro–Fertilized Embryos in Cattle. PLoS One *7*, e36627. https://doi.org/10.1371/JOURNAL.PONE.0036627.

71. Sigalos, G.A., Triantafyllidou, O., and Vlahos, N.F. (2016). Novel embryo selection techniques to increase embryo implantation in IVF attempts. Arch. Gynecol. Obstet. *294*, 1117–1124. https://doi.org/10.1007/S00404-016-4196-5.

72. ESHRE PGT-SR/PGT-A Working Group; Coonen, E., Rubio, C., Christopikou, D., Dimitriadou, E., Gontar, J., Goossens, V., Maurer, M., Spinella, F., Vermeulen, N., and De Rycke, M. (2020). ESHRE PGT Consortium good practice recommendations for the detection of structural and numerical chromosomal aberrations. Hum. Reprod. Open *2020*, hoaa017. https://doi.org/10.1093/HROPEN/HOAA017.

73. Caroselli, S., Figliuzzi, M., Picchetta, L., Cogo, F., Zambon, P., Pergher, I., Girardi, L., Patassini, C., Poli, M., Bakalova, D., et al. (2023). Improved clinical utility of preimplantation genetic testing through the integration of ploidy and common pathogenic microdeletions analyses. Hum. Reprod. *38*, 762–775. https://doi.org/10.1093/HUMREP/DEAD033.

74. Rubio, I., Kuhlmann, R., Agerholm, I., Kirk, J., Herrero, J., Escribá, M.J., Bellver, J., and Meseguer, M. (2012). Limited implantation success of direct-cleaved human zygotes: a time-lapse study. Fertil. Steril. *98*, 1458–1463. https://doi.org/10.1016/J.FERTNSTERT.2012.07.1135.

75. Treff, N.R., Krisher, R.L., Tao, X., Garnsey, H., Bohrer, C., Silva, E., Landis, J., Taylor, D., Scott, R.T., Woodruff, T.K., and Duncan, F.E. (2016). Next generation sequencing-based comprehensive chromosome screening in mouse polar bodies, oocytes, and embryos. Biol. Reprod. *94*, 76. https://doi.org/10.1095/BIOLREPROD.115.135483/2434387.

76. Chen, S., Zhou, Y., Chen, Y., and Gu, J. (2018). fastp: an ultra-fast all-in-one FASTQ preprocessor. Bioinformatics *34*, i884–i890. https://doi.org/10.1093/BIOINFORMATICS/BTY560.

77. Martin, M. (2011). Cutadapt removes adapter sequences from high-throughput sequencing reads. EMBnet. J. *17*, 10–12. https://doi.org/10.14806/EJ.17.1.200.

78. Garrison, E., and Marth, G. (2012). Haplotype-based variant detection from short-read sequencing. Preprint at arXiv. https://doi.org/10.48550/arXiv.1207.3907.

79. Anders, S., Pyl, P.T., and Huber, W. (2015). HTSeq—a Python framework to work with high-throughput sequencing data. Bioinformatics *31*, 166–169. https://doi.org/10.1093/BIOINFORMATICS/BTU638.

80. Hao, Y., Stuart, T., Kowalski, M.H., Choudhary, S., Hoffman, P., Hartman, A., Srivastava, A., Molla, G., Madad, S., Fernandez-Granda, C., and Satija, R. (2023). Dictionary learning for integrative, multimodal and scalable single-cell analysis. Nat. Biotechnol. *42*, 293–304. https://doi.org/10.1038/s41587-023-01767-y.

81. Van de Sande, B., Flerin, C., Davie, K., De Waegeneer, M., Hulselmans, G., Aibar, S., Seurinck, R., Saelens, W., Cannoodt, R., Rouchon, Q., et al. (2020). A scalable SCENIC workflow for single-cell gene regulatory network analysis. Nat. Protoc. *15*, 2247–2276. https://doi.org/10.1038/s41596-020-0336-2.

82. Wydooghe, E., Vandaele, L., Piepers, S., Dewulf, J., Van den Abbeel, E., De Sutter, P., and Van Soom, A. (2014). Individual commitment to a group effect: strengths and weaknesses of bovine embryo group culture. Reproduction *148*, 519–529. https://doi.org/10.1530/REP-14-0213.

83. Macaulay, I.C., Teng, M.J., Haerty, W., Kumar, P., Ponting, C.P., and Voet, T. (2016). Separation and parallel sequencing of the genomes and transcriptomes of single cells using G&T-seq. Nat. Protoc. *11*, 2081–2103. https://doi.org/10.1038/nprot.2016.138.

84. Li, H. (2013). Aligning sequence reads, clone sequences and assembly contigs with BWA-MEM. Preprint at arXiv. https://doi.org/10.6084/M9.FIGSHARE.963153.V1.

85. Liu, D. (2019). Algorithms for efficiently collapsing reads with Unique Molecular Identifiers. PeerJ *7*, e8275. https://doi.org/10.7717/PEERJ.8275.

86. Dobin, A., Davis, C.A., Schlesinger, F., Drenkow, J., Zaleski, C., Jha, S., Batut, P., Chaisson, M., and Gingeras, T.R. (2013). STAR: ultrafast universal RNA-seq aligner. Bioinformatics *29*, 15–21. https://doi.org/10.1093/BIOINFORMATICS/BTS635.

87. Graf, A., Krebs, S., Zakhartchenko, V., Schwalb, B., Blum, H., and Wolf, E. (2014). Fine mapping of genome activation in bovine embryos by RNA sequencing. Proc. Natl. Acad. Sci. USA *111*, 4139–4144. https://doi.org/10.1073/PNAS.1321569111.

STAR★METHODS

KEY RESOURCES TABLE

REAGENT or RESOURCE	SOURCE	IDENTIFIER
Biological samples		
Bovine embryos	Ghent University	N/A
Critical commercial assays		
Agencourt AMPure XP beads	Beckman Coulter, USA	Cat# A63881
REPLI-g SC kit	Qiagen, Germany	Cat# 150345
Deposited data		
GBS and single-cell RNA sequencing data reported in this paper	This paper	PRJEB76932
Software and algorithms		
fastp (v0.23.2)	Chen et al.[76]	https://github.com/OpenGene/fastp
cutadapt (v 1.18)	Martin et al.[77]	https://pypi.org/project/cutadapt/1.18/
freebayes (v 1.3.2)	Garrison et al.[78]	https://github.com/freebayes/freebayes
HTSeq (v 0.9.1)	Anders et al.[79]	https://github.com/simon-anders/htseq
Seurat (v5.0.1)	Hao et al.[80]	https://github.com/satijalab/seurat
Slingshot (v2.10.0)	N/A	https://github.com/kstreet13/slingshot
pySCENIC (v0.12.1)	Sande et al.[81]	https://github.com/aertslab/pySCENIC
R (v4.3.2)	N/A	https://www.r-project.org/

EXPERIMENTAL MODEL AND STUDY PARTICIPANT DETAILS

Ovaries were obtained post-mortem from 4- to 5-year-old cows at a commercial slaughterhouse. IVF was performed using commercial semen straws from a 5-year-old bull (CRV, Netherlands).

METHOD DETAILS

Single-cell collection from bovine blastomere outgrowths

In vitro *embryo production*

Standard *in vitro* procedures were followed to produce bovine embryos.[82] Briefly, bovine (*Bos taurus*) ovaries were collected and processed within 2 h. The ovaries were rinsed three times in warm physiological saline supplemented with 0.25μg/mL kanamycin. Using an 18-G needle and a 10-mL syringe, antral follicles (2 – 8 mm diameter) were punctured and kept separately per ovary in 2.5 mL Hepes-Tyrode's albumin-pyruvate-lactate (Hepes-TALP). Using a stereomicroscope, cumulus-oocyte complexes were collected and washed in Hepes-TALP and then in maturation medium (modified bicarbonate-buffered TCM-199 supplemented with 50 ppm gentamicin and 20 ng/mL epidermal growth factor). Cumulus-oocyte complexes were *in vitro* matured per donor in four-well dishes (NuncTM) in 500 μL maturation medium for 22 h at 38.5°C in 5% CO_2 in humidified air. *In vitro* fertilization was performed with frozen-thawed semen from a Holstein-Friesian bull (*Bos taurus*) after selection over a discontinuous 45/90% Percoll® gradient (GE Healthcare Biosciences, Uppsala, Sweden). The mature oocytes were fertilized by incubating them with spermatozoa at a concentration of 1 × 10^6 spermatozoa/mL in IVF–TALP medium enriched with BSA (Sigma A8806; 6 mg/mL) and heparin (20 μg/mL) for 21 hours at 38.5°C, 5% CO_2 in humidified air. After fertilization, the presumed zygotes were vortexed in 2.5 mL HEPES-TALP for 3 minutes to remove the cumulus and sperm cells adhered to the *zona pellucida* and subsequently transferred to 50 μL droplets of synthetic oviductal fluid (SOF), enriched with 4 mg/mL BSA (Sigma A9647), non-essential and essential amino acids (SOFaa), 5 μg/mL insulin, 5 μg/mL transferrin, and 5 ng/mL selenium. The droplets were covered with 900 μL paraffin oil (SAGE oil for tissue culture, ART-4008-5P, Cooper Surgical Company). *In vitro* culture was performed at 38.5°C in 5% CO_2, 5% O_2, and 90% N_2.

Blastomere dissociation and culture

The presumptive zygotes were monitored from 26 to 36 hours post-fertilization (hpf) every 30 minutes to identify a direct cleavage of the zygote into three or four blastomeres (multipolar division) or into two blastomeres (bipolar division). This time window was chosen based on our pilot study using time-lapse microscopy, which showed that most zygotes had cleaved within this period without progressing to a second cleavage. Blastomeres from embryos that cleaved into more than four cells or presented multiple fragments were not processed further. Immediately upon the first division, embryos were washed in Hepes-TALP and treated with 0.1%

pronase (protease from *S. griseus*) in TCM-199 to dissolve the *zona pellucida*. Next, the embryos were washed in TCM-199 with 10% FBS and then transferred to Ca^{+2}/Mg^{+2}-free PBS with 0.05% BSA to enhance blastomere dissociation, which was performed using a STRIPPER pipet holder and 170 μm and 135 μm capillaries (Origio, Cooper Surgical, CT, US) in Ca^{+2}/Mg^{+2}-free PBS supplemented with 0.1% polyvinylpyrrolidone (PVP). Subsequently, single blastomeres were washed in culture medium and transferred individually to one well of a Primo VisionTM micro well group culture dish (Vitrolife, Göteborg, Sweden), which contained a total of 16 small wells covered by a 40 μL droplet of culture medium and 3.5 mL paraffin oil. Single blastomeres were cultured at 38.5°C in 5% CO_2, 5% O_2, and 90% N_2 until 72, 121 or 170 hpf according to the experimental design.

Single-cell isolation

For isolation of single cells at 72 hpf, 121 hpf or from blastomeres that did not reach the blastocyst stage at 170 hpf, the outgrowths were transferred to Ca^{+2}/Mg^{+2}-free PBS with 0.1% PVP, and the cells were dissociated mechanically with a STRIPPER pipet holder and 170 μm and 135 μm capillaries (Origio, Cooper Surgical, CT, US). For blastomeres that reached the blastocyst stage at 170 hpf, single-cell isolation was done by incubating the embryos in trypsine-EDTA at 38.5°C, followed by washing in Ca^{+2}/Mg^{+2}-free PBS with 0.1% PVP, pipetting with a STRIPPER pipet holder, and 135 μm and 70 μm capillaries (Origio, Cooper Surgical, CT, US) and micromanipulation with holding (MPH-MED-35, Origio, Cooper Surgical, CT, US) and biopsy (MBB-BP-M-30, Origio, Cooper Surgical, CT, US) pipettes. When single-cell dissociation was not possible, clusters of cells were collected. Single cells from all time points were washed in Ca^{+2}/Mg^{+2}-free PBS with 0.1% PVP before transferring them into a well of a skirted 96-well plate (4ti-0960/C, AZENTA Life Sciences, Bioké, Leiden, The Netherlands) containing 2.5 μL of RLT lysis buffer with a 70 μm capillary (Origio, Cooper Surgical, CT, US) and a STRIPPER pipet holder screwed on 0.5 μL. The collected samples were kept on ice during the whole procedure and then stored at −80°C.

DNA and RNA separation, library preparation and sequencing

Separation of DNA and RNA from single cells

The DNA and mRNA from single cells were separated following the genome and transcriptome sequencing (G&T-seq) protocol[83] on a robotic liquid-handling platform (Microlab STAR Plus, Hamilton). Specifically, the 96-well sample plate was positioned on the robot deck alongside (a) a plate for capturing poly-A mRNAs, containing 10μl per well of Dynabeads® MyOneTM Streptavidin C1 (Thermo Fisher Scientific) bound to biotinylated poly-dT oligos containing the SmartSeq2 primer sequence '5BioTinTEG/ -AAGCAGTGGTAT CAACGCAGAGTACTTTTTTTTTTTTTTTTTTTTTTTTTTTTTTVN' (IDT), (b) a plate for washing away DNA from the cell lysate supernatant, containing 25μl per well of G&T-wash buffer, and (c) an empty DNA destination plate. First, the cell lysate was mixed with biotinylated poly-dT beads and incubated for 20 min. Subsequently, beads bound to mRNA were pulled down using a low elution magnet (Alpaqua) for 2 min, and the supernatant was transferred to the DNA destination plate. Following this, the beads were subjected to two washes, each with 10μl of G&T wash buffer, and the supernatant was transferred to the DNA destination plate. The DNA destination plate, containing 37.5μl of G&T wash buffer, was then centrifuged for 1 min at 1000g and stored at -80°C.

RNA amplification, library preparation and sequencing

The plate containing poly-A mRNA-bound beads was processed using an adapted SmartSeq2 protocol with 20 PCR cycles. Subsequently, the amplified single-cell cDNA was purified using a 0.8:1 ratio of Agencourt AMPure XP beads (Analis), followed by washing with 80% ethanol and elution in water. Libraries were generated from the amplified cDNA according to the Nextera XT (Illumina) protocol with quarter volumes. These libraries were pooled and sequenced using single-end 50 sequencing on a HiSeq4000 Illumina sequencer, aiming at 1 million reads per sample. For a subset of blastocyst stage single cells, the libraries were resequenced paired-end 150 on a NovaSeq 6000 Illumina sequencer for more reads.

DNA amplification, GBS library preparation and sequencing

For each blastomere outgrowth, DNA from either individual single cell or several cells was used for GBS (with double enzyme restriction) processing. A sibling blastocyst was collected and processed together when available. Whole-genome amplification (WGA) was carried out using the REPLI-g SC kit (Qiagen, Germany) following the manufacturer's guidelines, with variations in reaction volumes (full or half) and an incubation period of 2-3 hours. The DNA separated from the single cells stored in G&T wash buffer (see before), was thawed on ice, centrifuged for 1 min at 1000g, purified with Agencourt AMPure XP beads (Beckman Coulter, USA), eluted in 4 μl of scPBS and processed following the REPLI-g SC kit (Qiagen, Germany) manufacturer's guidelines with an incubation time of 2h. Additionally, bulk DNA was extracted from ovarian tissue of the donor cows (mothers of the respective embryos), semen from the bull (father of the embryos), and blood from the parents of the bull (paternal grandparents of the embryos) using the DNeasy Blood and Tissue kit (Qiagen, Germany).

The whole-genome amplified DNA and bulk DNA were subjected to double restriction digestion with 8 units (U) of PstI-HF (R3140S, NEB) and 4U of CviAII (R0640L, NEB) enzymes (New England Biolabs, NEB, USA) combined with adapter ligation using 200-300 ng as an input DNA for each sample. The restriction-ligation reaction was performed in a total reaction volume of 15 μl, with a final concentration of 1X rCutSmart buffer (B6004S, NEB), 1mM ATP (P0756S, NEB) and 160U of T4 DNA Ligase (M0202L, NEB). Next, the double-sided size-selection was performed with Agencourt AMPure XP beads (Beckman Coulter, USA) and 7 cycles of PCR to amplify and barcode size-selected adapter-ligated fragments using Q5 High-Fidelity 2X Master Mix (NEB) and 0.5 μM primer mix with the following program. Subsequently, the libraries were purified with Agencourt AMPure XP beads (Beckman Coulter, CA, USA), equimolarly pooled and sequenced paired-end 150 on NovaSeq 6000 Illumina sequencer, with a target of 20-30 million reads per sample.

Data analysis

GBS data processing, haplotyping and aneuploidy profiling

The raw reads were processed using fastp (v0.23.2)[76] to trim adaptor sequences, filter out low-quality reads, remove UMI sequences and append them to read names. Next, cutadapt (v 1.18)[77] was applied to select reads that start with the internal barcode and trim off the barcode. Reads were then mapped to bovine reference genome bosTau9 (ARS-UCD1.2) using BWA-MEM (v0.7.17).[84] Next, UMICollapse[85] was used for collapsing duplicated reads with the same UMI, while accounting for sequencing/PCR errors. Across all samples, we obtained a median of 64 million mapped reads. After UMI deduplication, a median of 35 million mapped reads were retained (Table S2). Variant calling was performed with freebayes (v 1.3.2).[78] Initially, variants were called for the parents and phasing reference(s) (parental grandparents or a sibling blastocyst). Subsequently, the identified variants were utilized as input to call variants for each single/multi-cell sample. The called SNVs were converted into bi-allelic calls (e.g., AA, AB, and BB) with B-allele frequency (BAF) values calculated based on allele-specific depth of coverage using a custom R script. The genotype calls and BAFs were then used as input for the siCHILD pipeline (details in the method paper[24]). In brief, siCHILD performs pedigree-based haplotyping analysis. The parents were first phased using phasing reference(s). Subsequently, for specific combinations of phased parental genotypes, corresponding SNP BAF values of the sample of interest were retrieved and plotted on paternal and maternal haplarithms. Genome-wide parental haplotype inheritance can then be inferred through visual inspection of the genome-wide haplarithm plots.

In addition to haplotype information, the R package QDNAseq and custom scripts were applied to BAM files post-deduplication for aneuploidy profiling with a fixed bin size of 100kb. To quantify the extent of aneuploidy, the percentage of aneuploid autosomal regions was calculated for each sample. Specifically, bins with a segmentation logR value within $log\ 2(1/2)$) and $\log 2(3/2)$ were classified as normal, while all other bins were classified as abnormal. This normal range represents the expected range for diploid cells. Since detailed ploidy information is unavailable, the results should be interpreted with this limitation in mind. The percentage of aneuploid autosomal regions was calculated by summing up the length of all abnormal bins and dividing it by the size of all autosomes. Samples were categorized based on the percentage of aneuploid autosomal regions: $\leq$%1 as euploid, 1-5% as low-level aneuploidy, 5-10% as medium-level aneuploidy, and >10% as high-level aneuploidy. To determine chromosome X nullisomy status, the lengths of all bins on chromosome X with a segmentation logR value were aggregated. The fraction of the chromosome X region exhibiting nullisomy was determined by dividing this sum by the size of chromosome X. Samples with >95% nullisomy in the chromosome X region were classified as chromosome X nullisomy.

The haplotype composition and aneuploidy status of each blastomere outgrowth were determined using GBS results from a single-cell/multi-cell sample. A sample was considered anuclear if >60% and >10% of the reads mapped to the mitochondrial genome before and after UMI deduplication, respectively, with empty haplarithm and copy number plots. To infer an outgrowth to be anuclear, each cell in the outgrowth was individually checked and confirmed to be anuclear. To verify the presence of mitochondrial genomes in inferred anuclear biopsies and ascertain their maternal inheritance, we exclusively called variants on the mitochondrial genome across all inferred anuclear biopsies using Freebayes (v1.3.2)[78] and compared the called genotypes (Table S3).

Single-cell RNA sequencing data preprocessing

The raw reads were processed with fastp (v0.23.2)[76] to trim adaptor sequences and filter out low-quality reads. Subsequently, the reads were mapped to the bovine reference genome bosTau9 (ARS-UCD1.2) using STAR aligner (v 2.7.3)[86] with Ensembl annotations ARS-UCD1.2.105. Next, raw counts per cell were obtained using HTSeq (v 0.9.1).[79] Cells with fewer than 200,000 detected molecules or fewer than 2,000 expressed genes were excluded from further analysis, resulting in 446 cells out of 677 passing these quality control thresholds. The retained cells exhibited a median of 862,384 molecules and 7,272 genes detected per cell (Table S2). Counts were then normalized and scaled using R package Seurat (v5.0.1),[80] with mitochondrial transcripts excluded from the analysis.

Cell clustering, cell type identification and trajectory analysis

Cell clustering was performed based on the normalized and scaled transcriptome profiles using UMAP implemented in Seurat (v5.0.1). Subsequently, we assigned molecular cell stage labels to each cluster based on the expression of (a) known marker genes for ICM and TF (e.g. FN1, KDM2B for ICM, GATA3 for trophectoderm, etc.[39,40]); (b) genes first expressed at 4-cell stage (minor EGA) or 8-16 cell stage (major EGA) in bovine embryos.[87] For trajectory analysis, we employed the R package Slingshot (v2.10.0) to infer developmental trajectories based on transcriptome profiles.

Regulon analysis

Regulon analysis was performed on the transcriptome data using pySCENIC (v0.12.1).[81] First, for each motif in the public collection (https://resources.aertslab.org/cistarget/motif_collections/), genes in the bovine reference genome bosTau9 (ARS-UCD1.2) with orthologs in humans were prioritized. This prioritization was determined by a scoring system that assessed the presence of the motif within a 10kb window upstream and downstream of the transcription start site. Consequently, a motif x gene matrix was generated. Next, this matrix served as input alongside the raw count matrix to pySCENIC (v0.12.1) to detect active regulons. pySCENIC was run ten separate times, and only regulons appearing two or more times were retained. The final AUC matrix was constructed using the maximum AUC values for each regulon among all runs in which they were present. The AUC heatmap was created with AUC values scaled for each regulon. To rank the identified regulons according to their specificity in each cell lineage, a regulon specificity score was calculated using "calcRSS" function within R package SCENIC (v 1.3.1). To identify the key regulons for each molecular stage, we considered only regulons where corresponding TFs were expressed in more than 50% of the cells. From these, for each stage, we selected the top 6 regulons with the most frequent TF expression among those ranked in the top 20 for both activity and specificity.

Differential expression and regulon analysis

Differential expression analysis was performed by comparing androgenetic/gynogenetic/polyploid cells to biparental diploid cells within each molecular cell stage using the FindMarkers function in Seurat (v5.0.1), employing the "MAST" method with a minimum percentage threshold of 0.5. Pseudotime values and aneuploid status were incorporated as latent variables in the model. Genes were considered differentially expressed if they met the criteria of an adjusted p-value < 0.05 and an absolute log2 fold change greater than 1. Differential regulon analysis was performed between cells exhibiting WG abnormalities and biparental diploid cells within each molecular cell stage by Wilcoxon ranked-sum test on the AUC values. Regulons were considered to have significantly different activity if they demonstrated an adjusted p-value < 0.05 and an absolute log2 fold change greater than 1. The functions of the differentially expressed genes and regulons were curated through manual online searches and literature reviews.

QUANTIFICATION AND STATISTICAL ANALYSIS

Categorical data were compared using the chi-squared test, with Fisher's exact test applied when cell counts were too small. Pseudotime values and percentages of mitochondrial transcripts were compared using Student's t-test. Statistical significance was determined using a two-tailed approach with a significance threshold of $p < 0.05$. All tests were conducted in R (v4.3.2). The numbers of cells/outgrowths/embryos are provided in the corresponding results description, figures and figure legends.